General Disclaimer

One or more of the Following Statements may affect this Document

- This document has been reproduced from the best copy furnished by the organizational source. It is being released in the interest of making available as much information as possible.

- This document may contain data, which exceeds the sheet parameters. It was furnished in this condition by the organizational source and is the best copy available.

- This document may contain tone-on-tone or color graphs, charts and/or pictures, which have been reproduced in black and white.

- This document is paginated as submitted by the original source.

- Portions of this document are not fully legible due to the historical nature of some of the material. However, it is the best reproduction available from the original submission.

NASA CONTRACTOR REPORT 166517

Flight Directors for STOL Aircraft

U.H. Rabin

NASA Grant NCC2-106
May 1983

NASA

NASA CONTRACTOR REPORT 166517

Flight Directors for STOL Aircraft

Uri H. Rabin
Department of Aeronautics and Astronautics
Stanford University
Stanford, California 94305

Prepared for
Ames Research Center
Under NASA Grant NCC2-106

National Aeronautics and
Space Administration

Ames Research Center
Moffett Field, California 94035

ABSTRACT

In this study we develop flight director logic for flight path and airspeed control of a powered-lift STOL aircraft in the approach, transition, and landing configurations. Two methods for flight director design are investigated. The first method is based on the Optimal Control Model (OCM) of the pilot. The second method, proposed here, uses a fixed dynamic model of the pilot in a state space formulation similar to that of the OCM, and includes a pilot work-load metric.

Several design examples are presented with various aircraft, sensor, and control configurations. These examples show the strong impact of throttle effectiveness on the performance and pilot work-load associated with manual control of powered-lift aircraft during approach. Improved performance and reduced pilot work-load can be achieved by using direct-lift-control to increase throttle effectiveness.

Flight path regulation in the presence of turbulence, glide-slope capture, and acceptable response to horizontal windshear, can be achieved, equally well, by both methods. The second design method provides improved control logic for manual control tasks by reducing the pilot's work-load. It is also easier to use and validate, and it can accommodate any linear model of the pilot.

ACKNOWLEDGEMENTS

I wish to express my gratitude to my advisor, Professor Arthur E. Bryson, Jr., for his guidance, advice, and encouragement throughout my graduate studies and during this research.

I also wish to thank William S. Hindson, who initiated this project, for the insight and helpful suggestions which he provided during long hours of discussions.

The support of the National Aeronautics and Space Administration under NASA-Ames grant NCC 2-106, is gratefully acknowledged.

For sharing the years of this research, for the understanding and support provided by Carol Fox, the deepest appreciaion is expressed.

This thesis is dedicated to my mother and late father, who taught me the value of education.

LIST OF SYMBOLS

A_y	output weighting matrix
b	wing span
B	control weighting matrix
d	vertical position perturbation from glide-slope
e	tracking error
f_i	fractional attention to cockpit indicator i
F	state matrix
G	control distribution matrix
h	altitude
H	output distribution matrix
i	input forcing function
k	DLC gain
K_c	controlled-element gain
K_p	pilot gain
J	cost function
L	turbulence integral scale
q	pitch rate
Q	process noise covariance matrix
R	measurement noise covariance matrix
s	Laplace operator
S	wing area
T_e	engine time constant
T_i	pilot lag time constant

T_n	pilot neuromuscular time constant
T_u	horizontal wing gust time constant
T_w	vertical wing gust time constant
u	horizontal speed perturbation
u	control vector
u_a	airspeed perturbation
u_w	horizontal wind gust
w	vertical speed perturbation
w_w	vertical wind gust
x	state vector
$X_{(\,)}$	axial force derivative
y	output vector
Y_c	controlled-element transfer function
Y_p	pilot transfer function
Y_{sol}	system open-loop transfer function
$Z_{(\,)}$	vertical force derivative

Greek :

γ	flight path angle
Γ	process noise distribution matrix
δ_e	engine speed
δ_s	stabilator deflection
δ_{sp}	spoiler deflection
δ_t	throttle deflection
δ_t^*	throttle command
δ_{tb}	throttle internal state
η	process noise vector

η_m	pilot motor noise vector
η_o	pilot observation noise vector
η_s	sensor noise vector
θ	pitch attitude
θ^*	pitch attitude command
θ_b	pitch attitude internal state
ρ	observation noise-to-signal ratio
τ	time delay
ϕ_m	phase margin
ω	radial frequency
ω_c	crossover frequency
ω_i	input forcing function bandwidth

Subscripts :

$()_i$	i-th component
$()_q$	pitch rate variable
$()_t$	throttle control variable
$()_u$	horizontal velocity variable
$()_w$	vertical velocity variable
$()_\theta$	pitch attitude control variable
$()_0$	initial or nominal value

Abreviations :

deg	degrees
ft	feet
kt	knots

lb	pounds
rms	root mean square
DLC	direct lift control
CTOL	conventional take-off and landing
LQG	linear quadratic gaussian
MIMO	multi-input multi-output
N/S	noise-to-signal
OCM	optimal control model of the pilot
PCAS	pitch control augmentation system
QSRA	Quiet Short-Haul Research Aircraft
SISO	single-input single-output
STOL	short take-off and landing
USB	upper surface blowing (flaps)

CONTENTS

LIST OF FIGURES

LIST OF TABLES

Chapter I

INTRODUCTION

1.1 BACKGROUND AND PURPOSE

Manual control of Short Take-Off and Landing (STOL) aircraft is generally more difficult than control of current Conventional Take-Off and Landing (CTOL) aircraft. Some of the difficulties are inherent : landing on a short field with acceptable sink rates requires more precise flight path and airspeed control, while stability and control effectiveness are reduced at low speeds.

The high lift coefficients necessary for STOL operation are generated by increased wing circulation and by thrust vectoring that results from blowing engine exhaust over specially designed trailing-edge flaps. Flight tests have shown [1,16] that powered-lift aircraft are characterized by : (1) sluggish flight path response to attitude changes, (2) operation on the backside of the drag curve (i.e., where drag increases when airspeed decreases), and (3) large changes in lift and drag with engine power setting. Both attitude and power changes produce significant changes in flight path angle and airspeed, which makes manual control difficult. In the approach and landing configurations, pitch attitude is used primarily for airspeed control, and thrust modulation is used primarily for flight path control. Exactly the opposite technique is used in the cruise configuration where the effect of controls is restored to that of conventional aircraft.

Most powered-lift aircraft incorporate a pitch-rate command/pitch-attitude hold augmentation system that effectively eliminates attitude control deficiencies [2,16]. The remaining problems, namely handling quality deficiencies associated with flight path and airspeed control, can be solved either by additional augmentation or by using a flight director.

The purpose of this study is to develop flight director logic for flight path and airspeed control of a powered-lift STOL aircraft in the the approach, transition, and landing configurations.

The function of a flight director is to process aircraft sensor data and to display to the pilot appropriate pitch attitude (or stabilator) and throttle commands. The flight director performs the cross-coupling and equalization that the pilot would otherwise have to provide. A flight director is less expensive than an autopilot, and provides the pilot with the training necessary for manual flight with conventional instruments. For this latter purpose, the usual status information (i.e., airspeed, radar altitude, glide-slope deviation etc.) are also displayed so that flight director failures can be detected, and the landing continued or aborted safely.

For the flight director to be effective it must provide satisfactory performance and produce acceptable pilot work-load. First, flight director control commands, if followed exactly by an ideal pilot, should result in the desired aircraft response. Second, the displayed commands should be compatible with human operator capabilities so that the pilot can track and execute the commands with acceptable levels of mental and

physical efforts. The last requirement implies knowledge about the human operator characteristics, which is the subject of manual control theory. Our knowledge about the pilot as a dynamic control component is far from being complete or even extensive, and notions such as "pilot work-load" still resist rigorous definition and treatment. Nevertheless, mathematical models of the pilot have proven useful in improving pilot/vehicle integration.

Two such models are relevant to this study. The crossover model [4] is the best known pilot-model for single-input single-output tracking tasks. Most of the research about pilot preference in controlled-element dynamics has been done with this model[4,5]. Several (single -input) flight directors were designed according to the results of this research which clearly indicated pilot preference for plant dynamics having k/s like characteristics. The second model, known as the Optimal Control Model (OCM) of the pilot [6], is inherently capable of treating multi-variable systems, and is used extensively in this study.

The first flight director design method investigated in this study is based directly on the OCM. This method has been used before [9], but the control configuration investigated there, a longitudinal hover task, is relatively uncoupled, and thus places less demand on the pilot than the STOL landing task investigated here. A second design method is proposed here, which includes consideration of the pilot work-load, and thus it should produce improved flight directors for manual control tasks. Several design examples are given to show the relative merits of the two design methods.

1.2 THESIS OUTLINE

Manual control theory is reviewed in Chapter II. The concept, structure, and special features of the OCM and crossover models are described. The aircraft and the control task are described in Chapter III. The Quiet Short-Haul Research Aircraft (QSRA) and its flight control system are presented, followed by a definition of the landing task and the associated aircraft configurations. The flight director design requirements, including design constraints and performance criteria, are given in the last section.

Two flight director design methods are presented in Chapter IV. The design procedure for each method is explained and the two methods are compared.

The pilot/vehicle mathematical model is developed in Chapter V. In Chapter VI, both design methods are used in design examples with various aircraft, sensor, and control configurations. Conclusions and recommendations for future research are given in the last chapter. Model parameters for the QSRA are included in Appendix A.

Chapter II

REVIEW OF MANUAL CONTROL THEORY

Until 1965 most of the research in the field of manual control was devoted to understanding the characteristics of the human operator as the controller of a single-input single-output (SISO) tracking task. The result was a set of quasi-linear models that predict human behavior quite well for these simple but important tasks. An excellent summary of this work can be found in the report by McRuer et al. [4]. Two approaches have been used to extend manual control theory to the multi-variable case. The first, using classical multiloop control theory, relies heavily on judgments concerning the closed-loop system structure, and consequently is difficult to use in a systematic fashion. The second, known as the Optimal Control Model of the pilot [6], uses state space methods and optimal control theory, and is inherently capable of treating multi-variable cases.

2.1 CLASSICAL MANUAL CONTROL

Classical manual control theory has been applied most successfully to time-invariant SISO compensatory tracking tasks. The model used to describe the pilot's behavior in these tasks is known as the crossover model [4]. The two essential elements of this model are (1) a describing-function analytical form, and (2) a set of adjustment rules which specify how to set the parameters of the model.

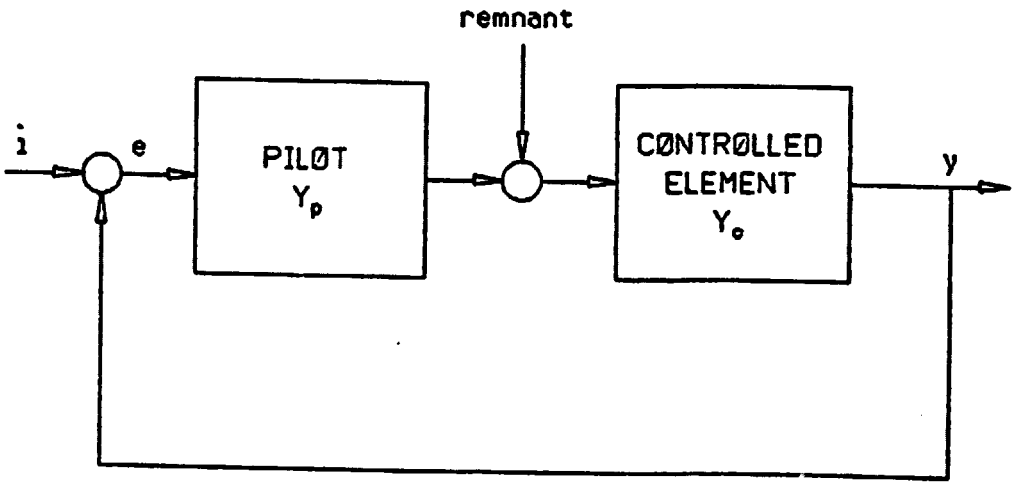

Figure 1: Block Diagram of a SISO Tracking Task

A typical SISO laboratory tracking task is illustrated in Figure 1. The pilot acts to minimize the displayed error, e, between the desired input, i, and the aircraft response y. The actuator, airframe, sensor and display dynamics are all included in the controlled-element dynamics represented by the transfer function $Y_c(s)$. The pilot is represented by the quasi-linear describing function $Y_p(j\omega)$. The remnant represents the non-linear part of the pilot behavior. The input forcing function, i, is modeled as a stationary random signal with Gaussian distribution, rms level σ_i, and bandwith ω_i.

The crossover model relates the form of the pilot equalization, Y_p, to the controlled-element dynamics, Y_c, by the equation :

$$Y_{sol}(j\omega) = Y_p(j\omega)Y_c(j\omega) = \frac{\omega_c e^{-j\omega\tau}}{j\omega} \quad \text{near } \omega_c \tag{2.1}$$

where

Y_{sol} is the <u>system</u> open-loop transfer function

ω_c is the crossover frequency (i.e., where $|Y_{sol}|$=0 dB.)

τ is the effective time delay representing transport lag and high frequency neuromuscular dynamics.

Eqn.(2.1) has as its basis a large body of experimental evidence [4,5]. Data from these experiments have shown that for a wide range of controlled-element dynamics such as $Y_c(s) = K_c$, K_c/s, and K_c/s^2, the above relationship can be satisfied with a pilot describing function of the form :

$$Y_p(j\omega) = K_p \frac{(T_1 j\omega+1)}{(T_i j\omega+1)} e^{-j\omega\tau} \tag{2.2}$$

where

K_p is the pilot gain

T_l is the lead time constant

T_i is the lag time constant

τ is the effective time delay

The crossover model predicts that, given the controlled-element dynamics Y_c, the pilot will adapt his behavior in the following way :

1. The lead and lag equalization, T_l and T_i, are adjusted by the pilot to achieve a -20 dB/decade slope in the system open-loop amplitude response ($|Y_{sol}|$) near or below the crossover frequency ω_c.

2. The pilot gain, K_p, is adjusted to locate the crossover frequency $\omega_c = K_p K_c$ above the input forcing function bandwidth ω_i so as to minimize tracking errors.

3. The pilot effective time delay, τ, is adjusted to provide adequate phase margin ϕ_m.

For the crossover model the phase margin is given by :

$$\phi_m = \pi/2 - \tau\omega_c$$

Experiments have shown that the operator tends to minimize the mean-square tracking error [4,5]. For a rectangular input spectrum of bandwidth ω_i and rms level σ_i, and under favorable tracking conditions ($\omega_c > \omega_i$), the rms tracking error is given by :

$$e^2/\sigma_i^2 \simeq \omega_i^2/(3\omega_c^2)$$

To decrease the rms tracking error the pilot tends to increase the crossover frequency ω_c by increasing his gain K_p. However the pilot time delay, τ, reduces the phase margin and usually limits ω_c to less then 10 rad/sec. To increase the phase margin the pilot can decrease his effective time delay by concentrating more on the task and increasing his neuromuscular tension. This represents an increased work load, and in any case the pilot's effective time delay cannot be reduced below some physiological limit, usually about 0.1 sec. When the pilot has to generate a low frequency lead, a larger time delay is incurred.

A substantial amount of research has been devoted to finding the relationship between the parameters of the crossover model and subjective pilot ratings used to describe flying qualities. Good correlation between these parameters would permit use of the crossover model to design for desirable aircraft handling characteristics. The results of this research have indicated that the best pilot ratings are obtained when the pilot equalization is minimal (i.e., no lead or lag is required). Only moderate degradations in ratings appear when lag or small values of lead are required. If larger values of lead equalization are required the pilot ratings degenerate rapidly [4].

2.2 THE OPTIMAL CONTROL MODEL OF THE PILOT

The Optimal Control Model (OCM) of the pilot is based on the assumption that a well-trained pilot has the ability to estimate the state of the aircraft, and to produce control actions that minimize the integral-square output errors with a constraint on integral-square control deflections. The main differences between the OCM and other

models of the human operator are the extensive use of state space concepts, the methods used to represent human limitations, and the use of modern control theory to compensate optimally for these limitations. The essential features of this model and the method of application are reviewed briefly in this section. A detailed description of the OCM concept can be found in the paper by Kleinman, Baron and Levinson [6].

2.2.1 Model Description

A block diagram of the closed-loop pilot-vehicle system is shown in Figure 2 [9]. Since the OCM method can handle multi-input multi-output (MIMO) systems, all the variables shown in the figure are vector quantities.

The displayed variables are assumed to be corrupted by an "observation noise" that accounts for the pilot's limitations in perceptual resolution and attention-sharing capacity. A Kalman filter is used to represent the pilot's ability to estimate the current state of the system. An optimal regulator is then synthesized to produce a set of control commands that minimize a quadratic performance index. The time delay element accounts for the pilot's central processing limitation. Just as observation noise is used to account for imperfect human perception, a "motor noise" is introduced to corrupt the optimal commands. This motor noise accounts for the pilot's inability to generate noise-free control actions and his imperfect knowledge of his own outputs. The last element of the OCM represents the bandwidth constraint of the neuromuscular system.

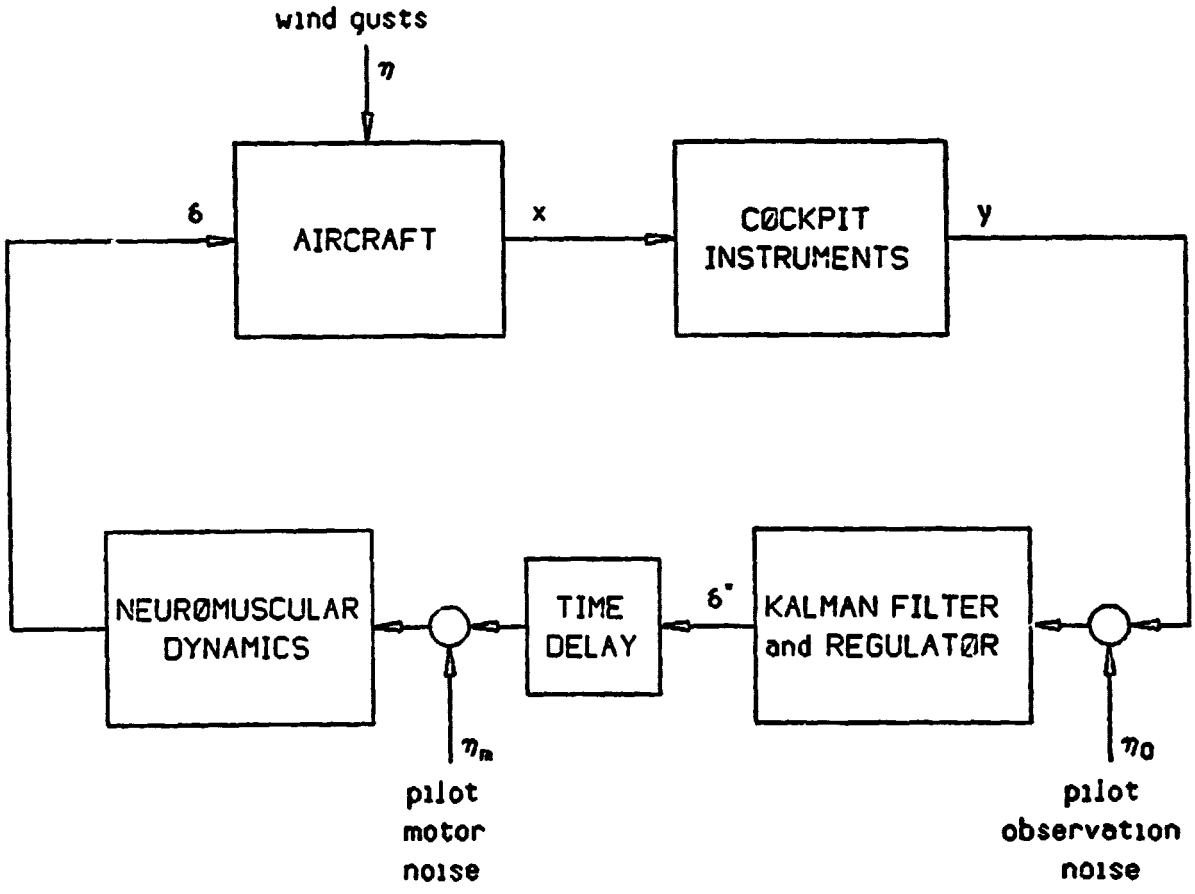

Figure 2: Block Diagram of the OCM

Human characteristics, as incorporated in the OCM, can be divided into four categories :

1. Task formulation.

2. Perceptual characteristics.

3. Central processing characteristics.

4. Neuromuscular actuation characteristics.

2.2.2 Task formulation

The pilot is assumed to adopt a strategy that minimizes a quadratic performance index of the form :

$$J = \frac{1}{2}\int_0^\infty (y^t A_y y + u^t B u)dt \qquad (2.3)$$

where A_y and B are weighting matrices associated with the displayed outputs y and the controls u. The elements of A_y relate to the performance objectives of the particular control task (e.g., glide-slope regulation), while those of B reflect the control utilization constraints that the pilot or the aircraft systems may impose. This strategy is based on an extension of SISO laboratory tracking tasks that showed that the operator tends to minimize rms output errors while using specified control energy [4,6]. The OCM formulation, using quadratic

performance indices, has been validated for both SISO tasks [6,8] and Multi-Input Multi-Output (MIMO) tasks [9,15].

2.2.3 Perceptual Characteristics.

The perceptual characteristics are modeled by :

$$y = Hx$$

$$y_p = y + \eta_o$$

where x is the state vector, y is the display vector, y_p is the vector of perceived variables, η_o is the observation noise vector, and H is the output distribution matrix. In formulating the display vector, it is assumed that the operator can extract both position and rate information from a single moving cockpit indicator [6].

The statistical properties of the observation noise are determined by:

1. Single observation.

   Studies of controller remnant have shown that the variance Q_{ii} of each white observation noise η_{oi} is proportional to the variance σ_i^2 of the associated perceived variable y_i. A normalized noise-to-signal (N/S) ratio of -20 dB (i.e., correlation time of 0.01 sec) is typically found in laboratory tracking tasks [7].

2. Task interference.

   In more complex situations, where several indicators are scanned by the pilot, the noise level is increased to account for the higher work-load. The scanning process appears to be highly complex and for most design applications a simplified form of task interference is used [11] :

$$\rho_i = \rho_0 / f_i$$

where ρ_0 is the basic noise-to-signal ratio used for a single indicator, f_i is the fraction of attention devoted to indicator i ($\Sigma f_i = 1.$), and ρ_i is the noise-to-signal ratio associated with indicator i. If attention is equally divided among all instruments, the noise to signal ratio will scale linearly with the number of indicators. Finally, it is assumed that the perception of the rate of change of the displayed variables is realized without additional attentional demand, and hence, f_i does not have to be decreased on this account.

2.2.4 Central Processing Characteristics

Central processing characteristics include the pilot's equalization and a time delay. The equalization element is the most important part of the model as it represents the pilot's ability to adapt his behavior to the dynamics of the aircraft. The pilot's equalization is modeled by a Kalman filter followed by a linear quadratic regulator. This implies that the pilot has an internal knowledge of both the dynamics of the system and the statistics of the disturbances.

A single time delay is used to represent the accumulated transport time lag associated with the central nervous system (visual, central processing, and neuromuscular transmission). Typical values are 0.15-0.25 sec [5,6].

2.2.5 Neuromuscular Actuation Characteristics

The OCM includes neuromuscular dynamics that account for physiological bandwidth limitations, and motor noise that accounts for the pilot's imperfect knowledge of his own outputs. Motor noise is also used to represent the pilot's inability to precisely produce the desired motions.

Neuromuscular dynamics are represented by a first order lag. Typically the neuromuscular time constant T_n is in the range 0.1-0.6 sec [4]. The neuromuscular dynamics can be modeled explicitly as part of the controlled-element dynamics. Alternatively, a control rate can be included in the performance index (eqn.(2.3)). The result is identical, but the explicit model eliminates the need to iterate the control rate weighting to achieve the desired value for T_n [6].

The motor noise is assumed to have the same form as the observation noise: the variance R_{ii} of each white motor noise η_{mi} is proportional to the variance σ_i^2 of the associated control u_i. In the experiments reported in [8], a normalized noise-to-signal ratio of -25 dB (i.e., correlation time of 0.005 sec) was typically obtained by model matching analysis.

Chapter III

AIRCRAFT AND TASK DESCRIPTION

3.1 AIRCRAFT DESCRIPTION

The Quiet Short-Haul Research Aircraft (QSRA) is currently being used by the NASA Ames Research Center for terminal area, low-speed, powered-lift flight research. The QSRA is a deHavilland C-8A Buffalo, modified by the Boeing Commercial Airplane Company to NASA specifications. It has a new wing and nacelles and four AVCO-Lycoming YF-102 engines mounted on top of the wing. The engines provide powered-lift by deflecting exhaust gases over four specially contoured trailing-edge flaps referred to as the upper surface blowing (USB) flaps. Lift is the sum of the usual wing lift, the normal component of the thrust vector that results from flow turning, and the aerodynamic supercirculation created by the engine exhaust flow over the wing's upper surface. The aircraft has a maximum gross weight of 55,000 lb and a wing area of only 600 square feet. Maximum trimmed lift coefficients in excess of 10 have been demonstrated in flight. STOL landings are made at a lift coefficient of 5.5 which results in landing speeds of only 65-75 knots, while still maintaining a substantial stall margin [2].

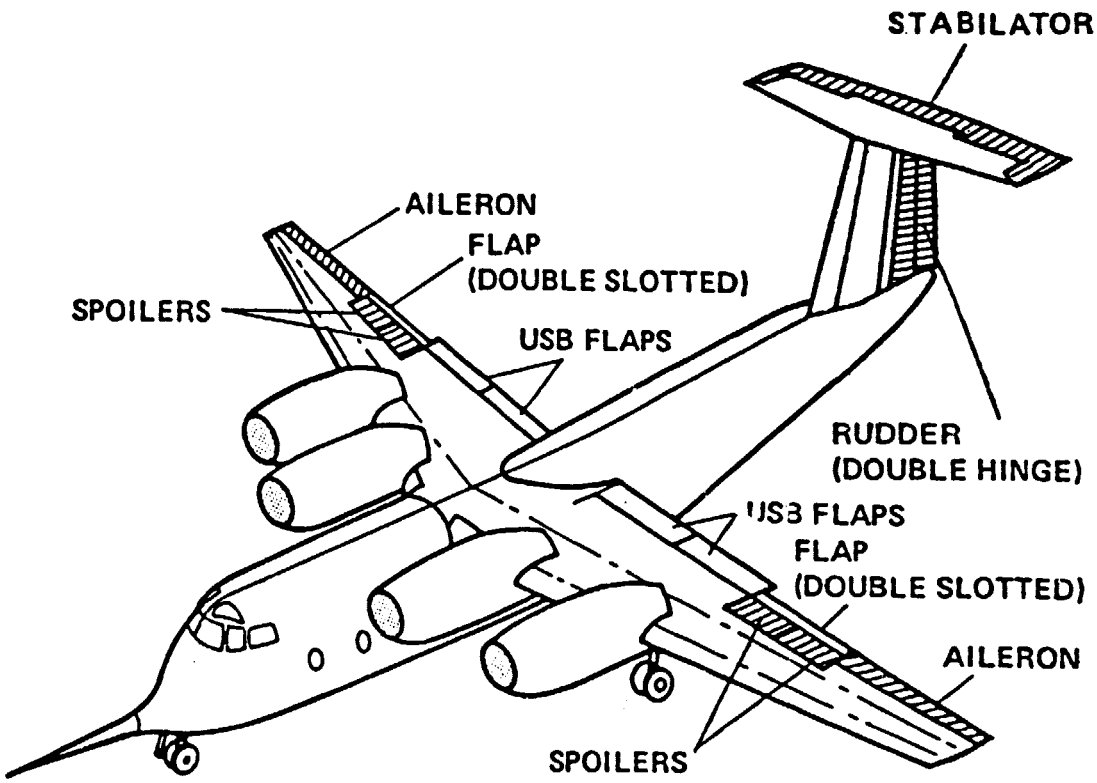

Figure 3: Flight-Control Surfaces

3.2 FLIGHT CONTROL SYSTEM

The airplane's control surfaces are identified in Figure 3. The primary flight controls consist of a stabilator, rudder, ailerons, spoilers and engine power. Secondary controls consist of four USB trailing-edge flaps and two conventional outboard trailing-edge flaps. A three-axis stability augmentation system is provided.

The use of the longitudinal controls is described below :

1. The USB flaps are used for configuration control. The USB flap deflection is usually 0-10 degrees for takeoff, 0 degrees for cruise, 30 degrees for initial approach and go-around, and 50 degrees for landing. USB flap deflection from 0 to 30 degrees is controlled by a handle in the overhead console. Flap deflections between 30 and 66 degrees are selected by a switch on the throttle which commands flap motion at a rate of 10 deg/sec. To enhance spanwise wing loading, the conventional outboard trailing-edge flaps are deflected to 59 degrees for all configurations except cruise.

2. Pitch control is achieved by stabilator deflection. When engaged, the pitch control augmentation system (PCAS) provides very tight rate command/attitude hold control. This type of pitch axis augmentation system is widely used on this class of aircraft and has the effect of increasing the short-period frequency and damping the phugoid mode. Attitude stabilization

is required in the approach configuration since changes in thrust or USB flap setting produce sizeable pitching moments.

3. Thrust is controlled by a throttle in the usual way, except that the orientation of the incremental thrust vector is strongly influenced by the USB flap setting as well as by the nominal power setting.

4. Direct-lift-control (DLC) is achieved by use of symmetric spoiler deflections commanded by an electric interconnect from the throttle. In this mode the spoilers are first biased up to a setting of 13 degrees and move from that nominal position in response to throttle movements. To ensure that authority is maintained, a washout is normally included. The higher bandwidth of the spoiler actuators and the increased effective control sensitivity result in faster flight-path response than can be obtained through the use of thrust modulation alone.

3.3 TASK DEFINITION

The tasks investigated in this study are the initial approach, transition, and landing phases of a powered-lift STOL aircraft. A typical approach and landing pattern for the QSRA is shown below :

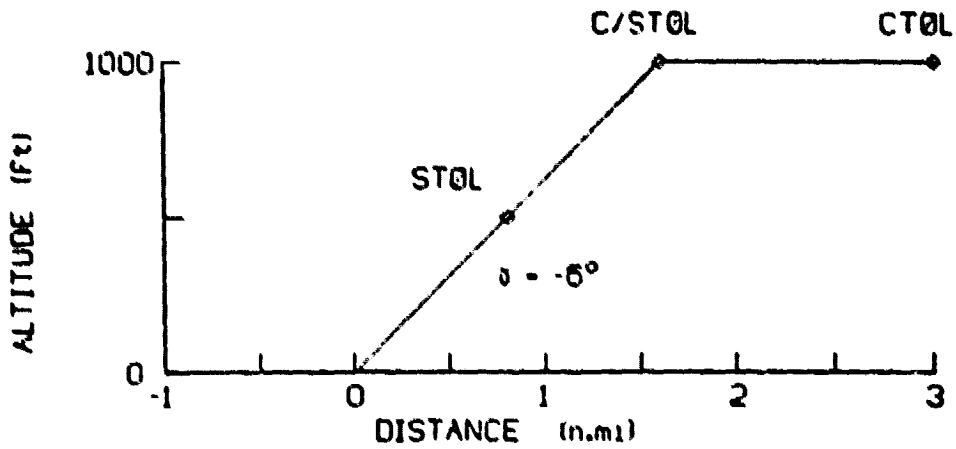

Three aircraft configuration/flight conditions are used to represent this task :

1. CTOL - A straight and level approach at an altitude of 1000 feet, and airspeed of 130 knots. The USB flaps are retracted.

2. C/STOL - In this transition configuration the USB flaps are deflected 30 degrees. The aircraft is on a six degrees glide-slope, at 90 kt.

3. STOL - For the landing configuration the USB flaps are deflected to 50 degrees. The aircraft is on the same glide-slope, at 70 kt.

The aircraft stability derivatives in the three configurations are given in Appendix A.

3.4 DESIGN REQUIREMENTS

The objective of this investigation is to develop flight director logic for flight path and airspeed control that will provide good performance with low pilot work-load in the approach and landing task described above. Special implementation considerations, such as simplifying the control laws for real-time operation, and display design, are not addressed.

3.4.1 Design Constraints

To conform to the standard utilization of controls, the flight director should provide only throttle and pitch attitude commands. (Pitch attitude command is used as a control input rather than stabilator deflection; this simplifies the logic and is a good approximation because of the high bandwidth of the pitch control augmentation system described earlier). The USB flaps and the conventional outboard flaps are held fixed at the appropriate setting for each configuration. The spoilers can be used, if necessary, only in the DLC mode in which they are linked to the throttle and so can be modulated without increasing the pilot's work-load. These design constraints also allow the flight director to be incorporated without any modification to the existing control mechanization.

3.4.2 Performance Criteria

Quantitative performance criteria are stated in terms of flight-path and control deviations from trim in the presence of random wind disturbances, and in terms of the control authority required to capture the glide-slope. These criteria are based on flight test data obtained with an aircraft similar to the QSRA [16].

1. Disturbance rejection.

   Horizontal and vertical wind gusts are approximated by shaping filters driven by white noise with rms outputs of 2.3 ft/sec. The average output and control deviations (in the rms sense) associated with these disturbances were chosen not to exceed the values shown in Table 1.

   To ensure satisfactory transient responses to wind gusts, additional criteria are used. The maximum values of flight path and control deviations following two-sigma horizontal and vertical wind gust impulses should not exceed those shown in Table 1.

2. Glide-slope capture.

   The capture of the glide-slope is represented by the aircraft response to an initial offset of 4 knots in airspeed or 20 feet in vertical position. Control deflections under these conditions were chosen not to exceed the maximum values specified in Table 1, and residual flight path deviations after 20 seconds should be less then 10% of the maximum values shown in the table. (The aircraft response to an initial offset in airspeed can also be regarded as the aircraft response to horizontal windshear).

3.4.3 Work-Load Criterion

Use of the flight director should reduce the pilot's work-load. A quantitative criterion is not specified. A metric for assessing pilot work-load is presented in Chapter IV.

TABLE 1

Flight-Path Regulation and Control Authority Criteria

variable		rms value	maximum value
u_a	[ft/sec]	2.25	6.75
d	[ft]	6.7	20.
$\dot{d}$	[ft/sec]	2.2	6.5
δ_t	[%]	3	6
θ	[deg]	2	4

Chapter IV

FLIGHT DIRECTOR DESIGN METHODS

Two methods for flight director control law design for a STOL aircraft are presented in this chapter. The first method, proposed by Levinson [10], uses the OCM concept to predict the equalization characteristics of a well-trained pilot performing the control task using only conventional cockpit instruments. These equalization characteristics, represented in the OCM formulation by a Kalman-filter/LQG regulator, are then used as the control laws for the flight director.

The second method, proposed here, uses a vehicle model which includes a flight director represented by a Kalman-filter/LQ regulator, and a fixed dynamic model of the pilot. This method was developed to overcome reservations about the first design method, in particular the lack of explicit design guidelines for reducing pilot work-load.

The two design methods are described below and then compared to each other.

4.1 FLIGHT DIRECTOR DISPLAY

A typical flight director display is shown in Figure 4.

The "director" part of the display includes :

1. Throttle command bar (a)
2. Pitch attitude command bar (b)

The "status" part of the display includes at least the following :

1. Aircraft symbol (c)
2. Artificial horizon with pitch attitude scale (d)
3. ILS box (glide-slope and localizer) (e)
4. Airspeed (f)
5. Radar altitude (g)
6. Sink-rate (h)

The status information enables the pilot to detect flight director failures, and to continue the flight safely.

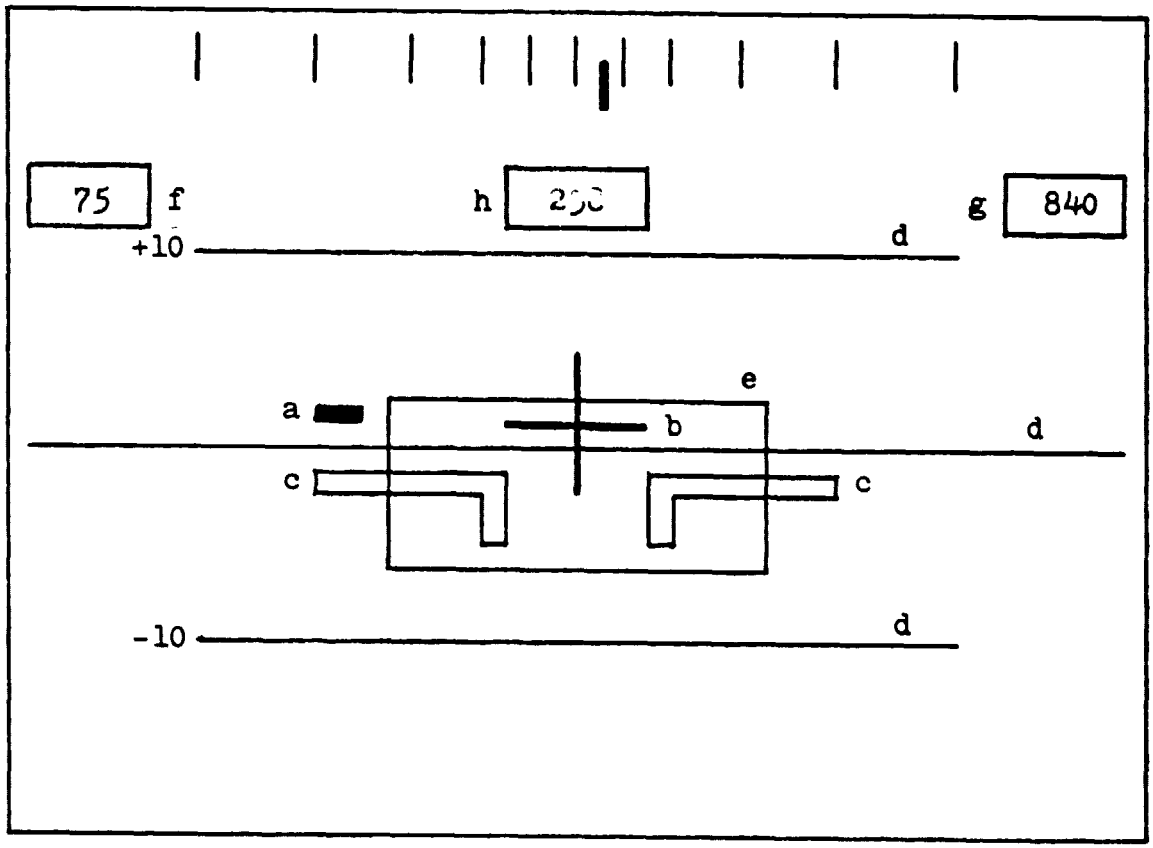

Figure 4: Flight Director Display

4. DESIGN METHOD I

Block-diagrams of the pilot/vehicle system for the design and implementation steps of method I are shown in Figure 5. For the design step, the pilot is assumed to be using conventional cockpit instruments (e.g., airspeed, sink-rate, and glide slope deviation indicators). Using the OCM concept as outlined in Section 3.2, the pilot's equalization characteristics are represented by the Kalman-filter/regulator block. The Kalman-filter and regulator are then regarded as a compensator, and are implemented, either directly or preferably in a simplified form, as the flight director control laws. Thus configured, the flight director will provide the same throttle and pitch attitude commands as would a well-trained pilot.

A point to note is that the pilot's time delay and neuromuscular dynamics are not included in the flight director control laws. These characteristics are assumed to be task-invariant and will be "supplied" by the pilot regardless of the form of the display compensation. On the other hand, including the time delay and neuromuscular dynamics in the model used for the design step, ensures that the resulting control laws will compensate "optimally" for these limitations.

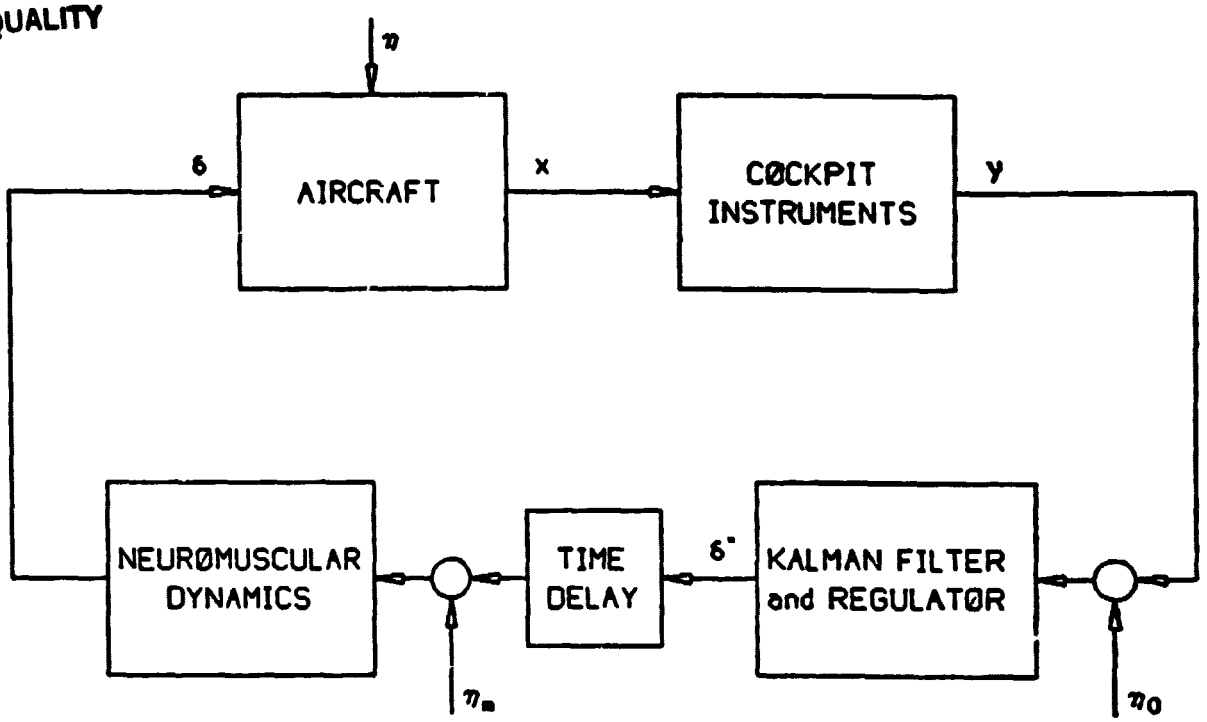

STEP 1 : DESIGN

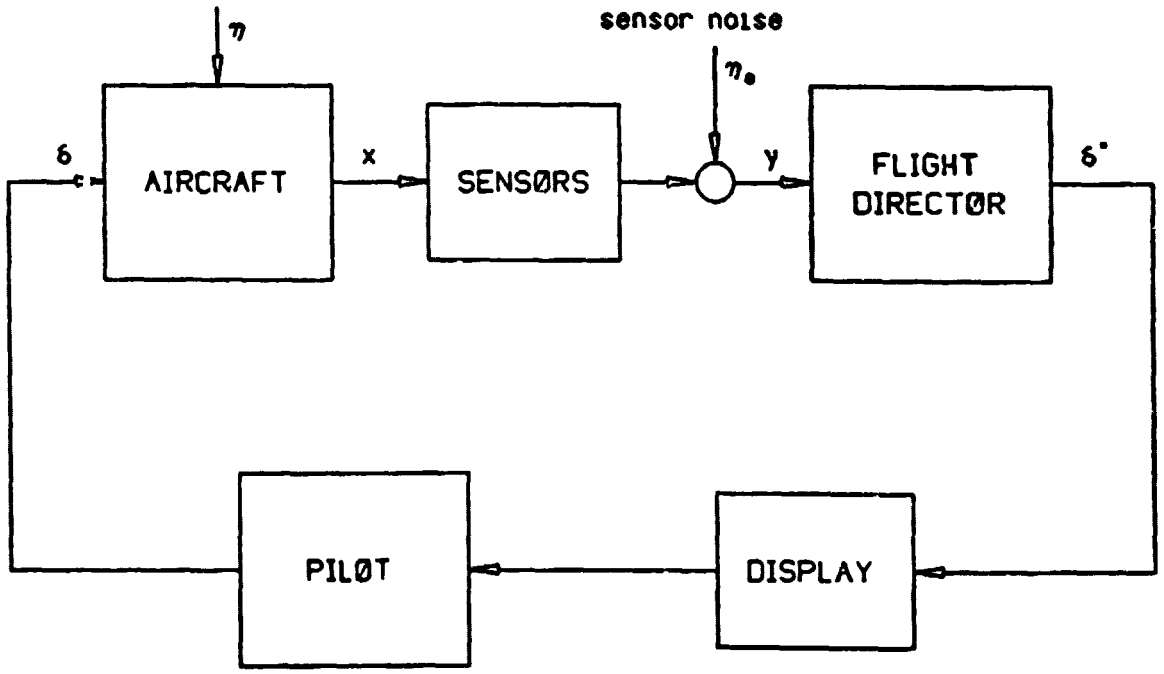

STEP 2 : IMPLEMENTATIØN

Figure 5: Pilot/Vehicle Block-Diagrams for Design Method I

4.2.1 Design Procedure

To satisfy both the OCM specifications and the flight director design criteria the following procedure is used :

1. A state space model of the pilot/vehicle system is set up according to the OCM formulation (c.f. Chapter V for modeling details).

2. Appropriate values for the output and control weighting matrices, A_y and B, of the cost function J (eqn.(2.3)) are selected to reflect the objectives of the control task. This subject will be discussed below.

3. Initial values for the spectral density matrices, Q and R (the pilot motor and observation noises) are determined. Given the wind gust statistics used in the model, expected values for the rms outputs and controls are assumed, based on aircraft characteristics and previous flight experience (e.g., the flight test data reported in [16]). These expected values are used to calculate the elements of Q and R that satisfy the OCM requirements for pilot motor and observation noise-to-signal ratios (c.f. Section 2.2.3).

4. The OCM is generated by computing the Kalman-filter and LQ regulator gains.

5. The spectral density matrices, Q and R, are adjusted, and step 4 is repeated until the specified noise-to-signal ratios are obtained.

6. The output and control weighting matrices, A_y and B, are adjusted, and steps 4 and 5 are repeated as necessary until the flight director design criteria, set forth in Section 3.4, are met.

Setting up the state space pilot/vehicle model and adjusting the matrices Q and R to achieve the specified noise-to-signal ratios is relatively straightforward. The essential problem is therefore the proper selection of the weighting matrices of the the cost function.

4.2.2 Selection of Weighting Matrices

In the design examples reported in [9] and [10], the weighting matrices were based on Bryson's rule [12]. Thus the diagonal elements of A_y and B are equal to the inverse of the square of the maximum allowable output deviations and control usage respectively. In both of these design examples the weighting matrices were held fixed, i.e., the last step of the design procedure presented above was not used. The design reported in [9] was evaluated in a piloted simulation which showed reasonable agreement between the rms outputs and controls predicted by the model and those obtained in the simulation. This evaluation also showed a definite reduction in rms outputs (and a smaller reduction in rms controls) for the flight director configuration compared to the

conventional display configuration and an improvement in pilot opinion ratings. For this study, using rms outputs and controls as the sole criterion was deemed insufficient, especially since a piloted simulation was not available to validate the design. Thus criteria based on closed-loop pilot/vehicle transient response were added (c.f. Section 3.4). The procedure for adjusting the weighting matrices to meet the criteria is presented in Chapter VI.

4.3 DESIGN METHOD II

A block-diagram of the pilot/vehicle system for design method II is shown in Figure 6. The vehicle model includes a flight director represented by the Kalman-filter/regulator block. The pilot is represented by a fixed dynamic model, with unity gain equalization, that is assumed to represent the lower work-load and improved pilot opinion associated with the use of a flight director. This pilot model is an extension of SISO manual control experimental results. These experiments have shown (c.f. Section 2.1) that the best pilot opinion ratings are obtained when the pilot equalization characteristics are minimal (i.e., unity gain equalization). If the flight director is well designed, the pilot's task is simply to transfer the two displayed commands to the two aircraft controls on a one-to-one basis, subject to his inherent time-delay and neuromuscular lag. Under these conditions it is assumed that the experimental results, although derived for a SISO task, are still useful design guidelines.

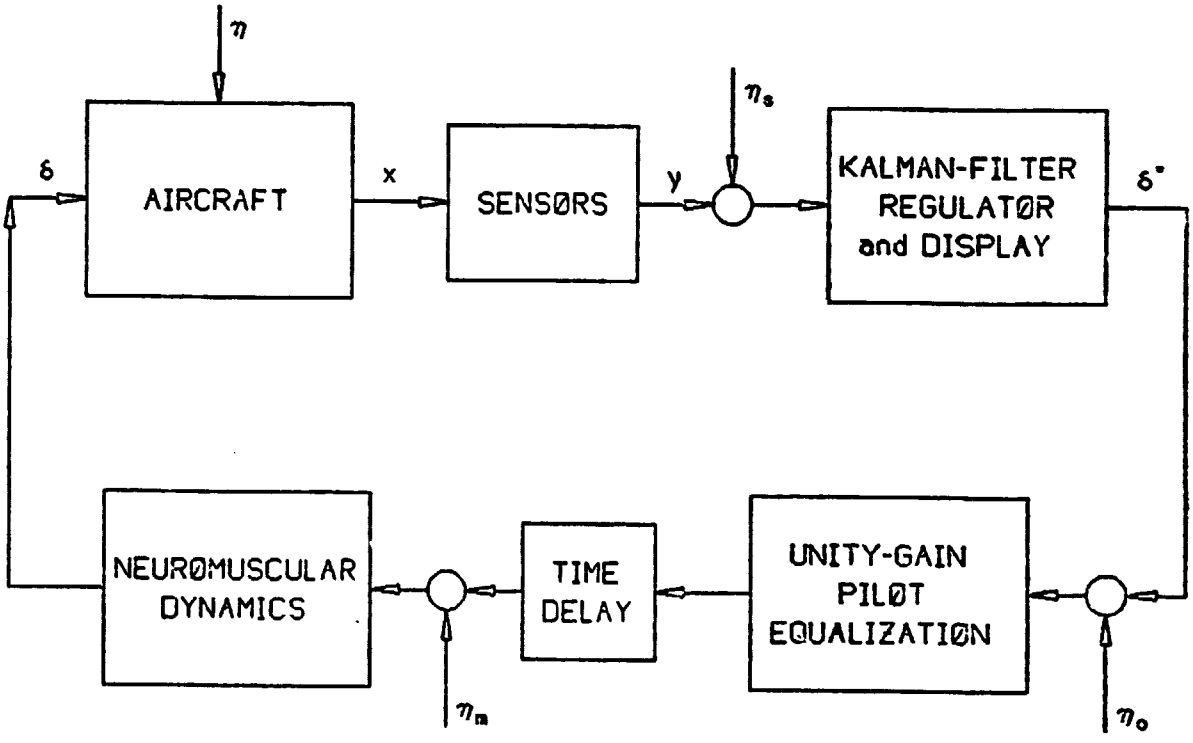

Figure 6: Pilot/Vehicle Block-Diagram for Design Method II

The pilot is thus represented by a unity gain equalization, followed by a time-delay and a neuromuscular lag that are modeled in the same way as in method I. The OCM formulation is also used to model the pilot observation characteristics with the following changes : (1) the observation noise levels are lower since only two variables are displayed to the pilot and consequently less scanning is required (c.f. Section 2.2.3), and (2) the pilot observation noise is treated as a process noise. Finally, sensor noise is introduced to corrupt the flight director inputs. (Sensor, or instrument noise was not included in the design model for method I since it is negligible compared to the pilot observation noise).

4.3.1 Work Load Metric

The pilot model used in method II is derived from a particular case (unity gain equalization) of the SISO crossover model (c.f. Section 2.1). According to the crossover model the pilot equalization characteristics and the controlled-element dynamics are related by the system open loop transfer function in eqn.(2.1). These experimental results indicate that the system open loop transfer function has a strong effect on the work-load associated with the control task. It is suggested here that the system open loop transfer functions will have a similar effect in MIMO systems. Experimental measurements of frequency response in MIMO systems are quite difficult and consequently the form of such a relationship has not been determined yet. (The validation of this design method in a piloted simulation may provide the answer). Therefore a modified form of eqn.(2.1) is used as a work-load metric :

for each control channel, the gain from the control input to the aircraft to the commanded control output of the pilot, should behave like k/s in the frequency range of interest. Cross transfer functions and phase characteristics are ignored.

Except for the additional work-load criterion, the design procedure for method II is the same as that used in method I and is not repeated here.

4.4 COMPARISON OF THE DESIGN METHODS

The second design method was developed to overcome reservations and possible deficiencies in using the first method. These reservations arose from the fact that design method I is unusual since the situation being modeled in the design stage is not the one in which the design will be used. Specifically, the flight director control laws are based on a model of a pilot perfoming a high work-load task using conventional cockpit displays. The Kalman-filter gains (and thus the flight director control laws) depend among other things on the pilot observation noise. The pilot observation noise levels postulated by the OCM are much higher than the sensor noises that are corrupting the flight director inputs. Thus, the Kalman-filter is designed for a measurement noise level much higher than the one it will actually experience. Another deficiency is that the first method does not include any mechanism to ensure a lower pilot work-load other than that implicit in the concept itself (i.e., a flight director control law that mimics the behavior of a well trained pilot is used).

A piloted simulation would normally be required to evaluate a flight director before actual implementation. However, this type of validation is not well suited to the several design cycles typically required in the development of advanced flight director systems. Instead, some method to permit a preliminary analytical validation is highly desirable. Since design method I is not based on the actual situation in which the design will be used, a separate analytical validation is especially desirable. Such a validation procedure obviously requires an analytical model of the pilot, and the one used in design method II is a possible candidate. Design method II is thus more efficient as the same mathematical model can be used for both the design and the validation phases and unnecessary design iterations are eliminated.

Another advantage of the second design method is that any (linear) model of the pilot can be used, whereas the first method is limited to the OCM. If further research in manual control theory results in a better understanding of the human operator, the improved model can be incorporated in design method II with only few modifications.

Chapter V

AIRCRAFT-PILOT MODEL DEVELOPMENT

In this chapter the pilot/vehicle state space model is developed. Most of the chapter is devoted to the development of the pilot/vehicle model for design method I. The modifications required for design method II are presented in the last section.

The pilot/vehicle model for design method I (c.f. Figure 2) includes the following :

1. A two degree-of-freedom translation model of the airframe.
2. A vertical and horizontal wind gust model.
3. A first order thrust model.
4. A fourth order model of the combined pilot time delay and neuromuscular systems.

These elements represent the open-loop plant. The pilot equalization process is represented by a Kalman-filter/regulator in the usual LQG formulation.

5.1 AIRFRAME STATE EQUATIONS

The linearized equations for longitudinal motion are :

$$\dot{u} = X_u u + X_w w - (g\cos\theta_0)\theta + X_e\delta_e + X_s\delta_s + X_{sp}\delta_{sp} - (X_u\cos\theta_0+X_w\sin\theta_0)u_w - (X_u\sin\theta_0+X_w\cos\theta_0)w_w \quad (5.1)$$

$$\dot{w} = Z_u u + Z_w w - (g\sin\theta_0)\theta + (U_0+Z_q)q + Z_e\delta_e + Z_s\delta_s + Z_{sp}\delta_{sp} - (Z_u\cos\theta_0+Z_w\sin\theta_0)u_w - (Z_u\sin\theta_0+Z_w\cos\theta_0)w_w \quad (5.2)$$

$$\dot{d} = -w + U_0\theta \quad (5.3)$$

$$\dot{\theta} = q \quad (5.4)$$

where

u,w are horizontal and vertical velocity perturbations

u_w,w_w are horizontal and vertical wind gusts

q,θ are pitch rate and angle

d is vertical perturbation from the glide-slope.

δ_s,δ_{sp} are stabilator and spoiler deflections

δ_e is engine speed

$X_{(\,)},Z_{(\,)}$ are axial and vertical force derivatives

U_0 is x-axis initial velocity component

θ_0 is initial pitch angle

Stability axes are used. The quantities u,u_w and X are defined positive forward, w,w_w and Z are positive downward; d is positive upward.

The pitching moment equation is not included in the above set since we have used the fact that the QSRA aircraft is equipped with a very tight pitch control augmentation system. This simplifies the aircraft control problem from three to two degrees of freedom. Consequently commanded pitch angle θ_a is regarded as the control input instead of δ_s, which can now be eliminated on the implicit assumption $\theta \approx \theta_a$. To eliminate the term $U_0\theta$ from the equations, $\dot{d} = -(w-U_0\theta)$ was used as a state variable instead of w.

The following usual assumptions were made to further simplify the equations :

- θ_0 small, thus $\cos\theta_0 \simeq 1$ and $\sin\theta_0 \simeq \theta_0$.
- Z_q small compared to U_0.
- $X_w \sin\theta_0 u_w$ etc. are negligible.
- The stabilator contributions to X and Z can be neglected.

With the above assumptions the airframe state equations are reduced to :

$$\dot{u} = X_u u - X_w \dot{d} + X_e \delta_e + X_{sp} \delta_{sp} + (X_w U_0 - g)\theta_a - X_u u_w - X_w w_w \qquad (5.5)$$

$$\ddot{d} = Z_u u - Z_w \dot{d} + Z_e \delta_e + Z_{sp} \delta_{sp} + (Z_w U_0 - g\theta_0)\theta_a - Z_u u_w - Z_w w_w \qquad (5.6)$$

Note : In the following, the subscript a of θ_a will be dropped.

5.2 TURBULENCE SHAPING FILTERS

Wind gusts are modeled as first order Markov processes. The relationship between the gust parameters and aircraft geometry, airspeed and altitude was taken from Holley and Bryson [14].

5.2.1 Horizontal wind gust (u_w)

$$u_w(s)/\eta_u(s) = 1/(T_u s+1)$$

or

$$\dot{u}_w = \frac{-u_w}{T_u} + \frac{\eta_u}{T_u} \qquad (5.7)$$

where

η_u = white noise with zero mean and spectral density Q_u

$Q_u = 2\sigma^2 L/C_1 V$

$T_u = L/C_1 V$

with

σ = rms(u_w) = 2.3 ft/sec

V = airspeed

L = turbulence integral scale = $L_\alpha h/(h_0+h)$

L_α = 2000 ft

h_0 = 2500 ft

b = wing span

$\beta = b/2L$

$$C_1 = \frac{(1+3\beta/2)^{2/3}}{1+3\beta}$$

5.2.2 Vertical wind gust (w_w)

The simplified form for small B was used to obtain a first order gust model :

$$\dot{w}_w = \frac{-w_w}{T_w} + \frac{\eta_w}{T_w} \qquad (5.9)$$

where

η_w = white noise with zero mean and spectral density Q_w

$Q_w = \sigma^2 L/V$

$T_w = L/2V$

5.3 THRUST MODEL

In the flight regime of interest the thrust is assumed to follow engine rotational speed linearly. The engine speed response to throttle position is modeled as a first order lag :

$$\dot{\delta}_e = \frac{-\delta_e}{T_e} + \frac{\delta_t}{T_e} \qquad (5.10)$$

where

δ_t = throttle position, in units of equivalent engine rpm

T_e = engine time constant

5.4 DIRECT LIFT CONTROL MECHANIZATION

In the DLC mode the spoilers are linked electricaly to the throttle. Thus :

$$\delta_{sp} = k\delta_t$$

5.5 PILOT TIME-DELAY AND NEUROMUSCULAR DYNAMICS SYSTEM

These two elements are connected as follow :

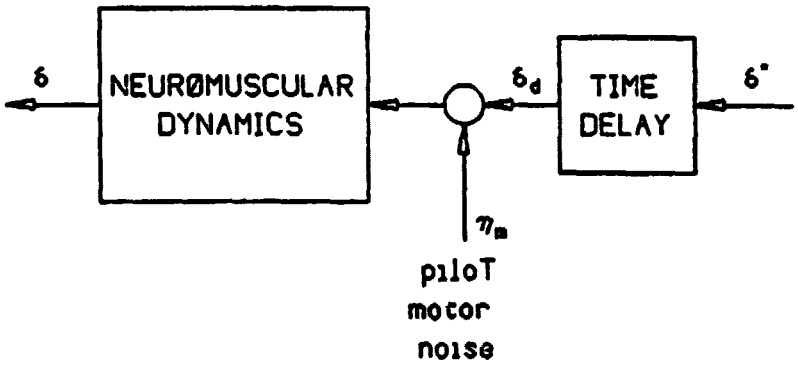

where

δ^* = desired control (regulator output)

δ_d = delayed control

δ = control input (to the aircraft)

η_m = pilot motor noise

The time-delay element is modeled by a Padé approximation :

$$\frac{\delta_d(s)}{\delta^*(s)} = \frac{-(s-2/\tau)}{(s+2/\tau)} \qquad (5.11)$$

The neuromuscular system is approximated by a first order lag :

$$\frac{\delta(s)}{\delta_d(s)+\eta_m(s)} = \frac{1/T_n}{s+1/T_n} \qquad (5.12)$$

The transfer function between the desired control and the actual control input is obtained by combining the two elements :

$$\delta(s) = \frac{-1/T_n(s-2/\tau)}{(s+1/T_n)(s+2/\tau)}\,\delta^*(s) + \frac{1/T_n}{(s+1/T_n)}\,\eta_m(s)$$

$$= \frac{-1/T_n(s-2/\tau)\delta^*(s) + 1/T_n(s+2/\tau)\eta_m(s)}{s^2 + (2/\tau+1/T_n)s + 2/(\tau T_n)} \qquad (5.14)$$

There are two such systems, one for the throttle channel (δ_t) and one for the pitch attitude control channel (θ). Transforming eqn. (5.14) into a state space form with the appropriate parameters for the throttle channel we get :

$$\begin{Bmatrix} \dot{\delta}_t \\ \dot{\delta}_{tb} \end{Bmatrix} = \begin{bmatrix} -(2/\tau_t+1/T_{nt}) & 1 \\ -2/(\tau_t T_{nt}) & 0 \end{bmatrix} \begin{Bmatrix} \delta_t \\ \delta_{tb} \end{Bmatrix} + \begin{bmatrix} -1/T_{nt} \\ 2/(\tau_t T_{nt}) \end{bmatrix} \delta_t^* + \begin{bmatrix} 1/T_{nt} \\ 2/(\tau_t T_{nt}) \end{bmatrix} \eta_{mt} \qquad (5.15)$$

And correspondingly for the pitch control channel :

$$\begin{Bmatrix} \dot{\theta} \\ \dot{\theta}_b \end{Bmatrix} = \begin{bmatrix} -(2/\tau_\theta+1/T_{n\theta}) & 1 \\ -2/(\tau_\theta T_{n\theta}) & 0 \end{bmatrix} \begin{Bmatrix} \theta \\ \theta_b \end{Bmatrix} + \begin{bmatrix} -1/T_{n\theta} \\ 2/(\tau_\theta T_{n\theta}) \end{bmatrix} \theta^* + \begin{bmatrix} 1/T_{n\theta} \\ 2/(\tau_\theta T_{n\theta}) \end{bmatrix} \eta_{m\theta} \qquad (5.16)$$

where

δ_{tb} = throttle channel internal state

θ_b = pitch channel internal state

τ_t = throttle channel time-delay

τ_θ = pitch channel time-delay

T_{nt} = throttle channel neuromuscular time constant

$T_{n\theta}$ = pitch channel neuromuscular time constant

5.6 PILOT/VEHICLE SYSTEM FOR DESIGN METHOD I

Combining the various elements, the following dynamic system is obtained (c.f., top of Figure 5) :

$$\dot{x} = Fx + Gu + \Gamma\eta$$

$$y = Hx + \eta_o$$

where

The state vector x is :

u	[ft/sec]	Horizontal inertial velocity
$\dot{d}$	[ft/sec]	Sink rate
d	[ft]	Vertical position
δ_e	[%]	Engine speed
δ_t	[%]	Throttle position
δ_{tb}	[%/sec]	Internal throttle state
θ	[deg]	Pitch attitude
θ_b	[deg/sec]	Internal pitch attitude state
u_W	[ft/sec]	Horizontal wind gust
w_W	[ft/sec]	Vertical wind gust

The control vector u is :

δ_t^*	[%]	Throttle command (regulator output)
θ^*	[deg]	Pitch command (regulator output)

The process noise vector η is :

η_u, η_w	Turbulence
$\eta_{mt}, \eta_{m\theta}$	Pilot motor noise

The output/observation vector y is chosen to be :

u_a	[ft/sec]	Airspeed
d	[ft]	Vertical position
$\dot{d}$	[ft/sec]	Sink rate
$\ddot{d}$	[ft/sec^2]	Vertical acceleration
u	[ft/sec^2]	horizontal acceleration

The associated observation noise vector is :

$\eta_{ou}, \eta_{od}, \eta_{o\dot{d}}, \eta_{o\ddot{d}}, \eta_{o\dot{u}}$.

Note : The actual number of outputs used in a given design may vary. See Chapter VI for details.

The state matrix is :

$$F = \begin{bmatrix} X_u & X_w & 0 & X_\theta & kX_{sp} & 0 & X_w U_0 - g & 0 & -X_u & -X_w \\ -Z_u & -Z_w & 0 & -Z_\theta & -kZ_{sp} & 0 & -Z_w U_0 + g\gamma_0 & 0 & Z_u & Z_w \\ 0 & -1. & 0 & 0 & 0 & 0 & 0 & 0 & 0 & 0 \\ 0 & 0 & 0 & -1/T_\theta & 1/T_\theta & 0 & 0 & 0 & 0 & 0 \\ 0 & 0 & 0 & 0 & -2/\tau_t + 1/T_{nt} & 1 & 0 & 0 & 0 & 0 \\ 0 & 0 & 0 & 0 & -2/(\tau_t T_{nt}) & 0 & 0 & 0 & 0 & 0 \\ 0 & 0 & 0 & 0 & 0 & 0 & -2/\tau_\theta + 1/T_{n\theta} & 1 & 0 & 0 \\ 0 & 0 & 0 & 0 & 0 & 0 & -2/(\tau_\theta T_{n\theta}) & 0 & 0 & 0 \\ 0 & 0 & 0 & 0 & 0 & 0 & 0 & 0 & -1/T_u & 0 \\ 0 & 0 & 0 & 0 & 0 & 0 & 0 & 0 & 0 & -1/T_w \end{bmatrix}$$

The output distribution matrix is :

$$H = \begin{bmatrix} 1 & 0 & 0 & 0 & 0 & 0 & 0 & 0 & -1 & 0 \\ 0 & 0 & 1 & 0 & 0 & 0 & 0 & 0 & 0 & 0 \\ 0 & 1 & 0 & 0 & 0 & 0 & 0 & 0 & 0 & 0 \\ X_u & X_w & 0 & X_\theta & kX_{sp} & 0 & X_w U_0 - g & 0 & -X_u & -X_w \\ -Z_u & -Z_w & 0 & -Z_\theta & -kZ_{sp} & 0 & -Z_w U_0 + g\gamma_0 & 0 & Z_u & Z_w \end{bmatrix}$$

Note : $k = 0$ if DLC is not used.

The control and process noise distribution matrices are :

$$G = \begin{bmatrix} 0 & 0 \\ 0 & 0 \\ 0 & 0 \\ 0 & 0 \\ -1/T_{nt} & 0 \\ 2/(\tau_t T_{nt}) & 0 \\ 0 & -1/T_{n\theta} \\ 0 & 2/(\tau_\theta T_{n\theta}) \\ 0 & 0 \\ 0 & 0 \end{bmatrix} \qquad \Gamma = \begin{bmatrix} 0 & 0 & 0 & 0 \\ 0 & 0 & 0 & 0 \\ 0 & 0 & 0 & 0 \\ 0 & 0 & 0 & 0 \\ 0 & 0 & 1/T_{nt} & 0 \\ 0 & 0 & 2/(\tau_t T_{nt}) & 0 \\ 0 & 0 & 0 & 1/T_{n\theta} \\ 0 & 0 & 0 & 2/(\tau_\theta T_{n\theta}) \\ 1/T_u & 0 & 0 & 0 \\ 0 & 1/T_w & 0 & 0 \end{bmatrix}$$

5.7 PILOT/VEHICLE SYSTEM FOR DESIGN METHOD II

The pilot/vehicle system for design method II is the same as the one for design method I except :

1. The aircraft outputs, instead of being displayed to the pilot, are used as input to the flight director.

2. Only two variables are displayed to the pilot : δ_t^* and θ^*. The pilot observation noise is now considered as a process noise.

Referring to Figure 6, the following system is obtained :

$$\dot{x} = Fx + Gu + \Gamma\eta$$

$$y = Hx + \eta_s$$

where

The process noise vector η is :

η_u, η_w	turbulence
$\eta_{mt}, \eta_{m\theta}$	pilot motor noise
$\eta_{ot}, \eta_{o\theta}$	pilot observation noise

The measurement (sensor) noise vector is :

η_{su}, η_{sd}, $\eta_{s\dot{d}}$, $\eta_{s\ddot{d}}$, $\eta_{s\dot{u}}$.

Only the process noise distribution matrix is different :

$$\Gamma = \begin{bmatrix} 0 & 0 & 0 & 0 & 0 & 0 \\ 0 & 0 & 0 & 0 & 0 & 0 \\ 0 & 0 & 0 & 0 & 0 & 0 \\ 0 & 0 & 0 & 0 & 0 & 0 \\ 0 & 0 & 1/T_{nt} & 0 & -1/T_{nt} & 0 \\ 0 & 0 & 2/(\tau_t T_{nt}) & 0 & 2/(\tau_t T_{nt}) & 0 \\ 0 & 0 & 0 & 1/T_{n\theta} & 0 & -1/T_{n\theta} \\ 0 & 0 & 0 & 2/(\tau_\theta T_{n\theta}) & 0 & 2/(\tau_\theta T_{n\theta}) \\ 1/T_u & 0 & 0 & 0 & 0 & 0 \\ 0 & 1/T_w & 0 & 0 & 0 & 0 \end{bmatrix}$$

Chapter VI

DESIGN EXAMPLES

Several flight director design examples are presented in this chapter. The first section describes the software tools used to generate these examples. The main design effort was a trade-off study on the number of aircraft sensors and the amount of control authority required. The STOL configuration was used in this study to gain insight about the two flight director design methods presented in Chapter IV. A practical procedure for satisfying the design criteria by iteration on the cost function weighting matrices was also established.

The trade-off study examples are presented in the following order :

1. Three sensors configuration - Baseline Characteristics : all performance criteria except one are met (insufficient throttle effectiveness is the limiting factor); pilot work-load level judged too high.

2. Five sensors configuration - Significant reduction in pilot work-load; small improvement in performance.

3. DLC configuration with three sensors - Significant improvement in performance due to increased throttle effectiveness; also pilot work-load is similar to that of the five sensors configuration but only three sensors were required.

The last section of this chapter includes a similar design example for the C/STOL configuration.

6.1 SOFTWARE TOOLS

A computer program, "OPTSYS", developed by the Department of Aeronautics and Astronautics at Stanford University, was used to determine the Kalman-filter and regulator gains [13]. The program was modified to calculate the pilot observation and motor N/S ratios, and to predict the appropriate values of the spectral density matrices Q and R that would result in the N/S ratios specified by the OCM method. With this modification, the specified N/S ratios could usually be obtained with only two iterations.

The original program provided a printout of rms states,controls, and outputs which were checked against the performance criteria (c.f. Section 3.4.2). The program was further modified to provide :

1. An output disk file containing the closed-loop state matrix computed by OPTSYS and the control distribution matrix. These matrices were used as input to a time response program written by the author. The time response printouts and plots were then compared to the performance criteria on wind gust rejection and glide-slope capture given in Section 3.4.2.

2. A printout and output disk file containing the system open-loop (Y_{sol}) frequency response from 0.1 to 100 rad/sec. These data were used to assess the pilot work-load and satisfy the additional criterion proposed for method II in Section 4.2.1.

6.2 PILOT PARAMETERS AND SENSOR NOISE

6.2.1 Pilot Parameters

The pilot time delay and neuromuscular lags used are :

$\tau_t = 0.15$ sec $\qquad \tau_\theta = 0.20$ sec

$T_{nt} = 0.20$ sec $\qquad T_{n\theta} = 0.25$ sec

6.2.2 Sensor Noise

The values chosen for the elements of R (for design method II only) are based on conservative estimates of typical aircraft sensor noise levels. The noise sources are independent, so R is diagonal and each element has the form :

$$R_{ii} = 2\tau_s\sigma_i^2$$

where σ_i is the rms noise level for sensor i, and the correlation time τ_s is chosen to be smaller than the sample interval for typical real-time Kalman-filter implementation.

The values used are :

$\tau_s = 0.025$ sec

$\sigma_{u_a} = 0.75$ ft/sec

$\sigma_d = 1.$ ft

$\sigma_{\dot{d}} = 0.5$ ft/sec

$\sigma_{\ddot{d}} = 0.2$ ft/sec^2

$\sigma_{\dot{u}} = 0.2$ ft/sec^2

6.3 TRADE-OFF STUDY

6.3.1 Three Sensors Configuration

Three sensors were used for the initial design example : airspeed (u_a), vertical position (d), and sink-rate ($\dot{d}$). In design method I these variables are displayed to the pilot by three cockpit instruments (c.f. Figure 5). The basic pilot observation N/S ratio (-20 dB) is multiplied by three to account for the scanning process, and results in an effective normalized N/S ratio of -15 dB. In design method II these three measurements are processed by the flight director, and only two variables are displayed to the pilot : throttle command (δ_t), and pitch attitude command (θ). The pilot observation noise level is therefore lower by one third (-17 dB).

An initial set of cost function weighting matrices was obtained by Bryson's rule (c.f. Section 4.1.2), based on the maximum errors specified in Table &limits.. The resulting flight directors, using either method, satisfied both the statistical and deterministic wind gust rejection criteria. The glide slope capture and pilot work-load criteria were not satisfied, and the pitch attitude control was felt to be under-utilized.

The adjustment procedure for the weighting matrices that evolved during this study is :

1. General - The pitch attitude weighting was used as reference and was not modified.

2. Performance criteria - The airspeed error (u_e) and vertical position error (d) weightings were increased in order to decrease the maximum and residual errors on u_e and d. The throttle weighting was increased to more nearly equalize the control utilization of the throttle and pitch attitude. The u_e and d weighting were increased accordingly to keep the same ratio of outputs to controls weighting. The sink rate weighting had a much smaller effect and was not modified.

3. Work-load criterion (method II only) - The effect of the weighting matrices on the work-load metric was more complicated. No analytical procedure is known to allow systematic shaping of the frequency response resulting from LQG design. Consequently trial and error adjustements of the weightings were made and the effects assessed. Taken individually, any weighting except the one on sink rate affected mostly the low frequency range of the system open-loop frequency response magnitude curve. Collectively, the previously described adjustments, required to improve the flight director performance, had a detrimental effect on the work-load metric. That is, improving performance resulted in the frequency response magnitude curves becoming steeper and farther away from the required -20 dB/decade slope. The work-load metric could be improved significantly only by increasing the sink rate weighting or decreasing the sink rate measurement noise. These adjustments provided relatively good control of the frequency response magnitude curve slope for the pitch attitude channel, but insufficient control of the corresponding curve for the throttle channel.

The adjustment procedure was carried out separately for the two design methods. The end result was two sets of weighting matrices : one for method I, the other for method II. The difference between the two sets was not significant, and only one set (the weighting matrices as adjusted for method II) was used to generate the design examples presented below.

Examples of flight director performance for the STOL configuration, using three sensors are presented in the first column of Tables 2 to 6, and in Figures 7 to 10.

As mentioned earlier, the wind gust rejection specifications were achieved. Table 2 shows the average outputs and controls in the presence of random wind gusts. Both methods produced similar results. Tables 3 and 4 show the aircraft response to a two-sigma impulse in horizontal and vertical wind gusts respectivly. A more detailed picture of the aircraft response is shown by the corresponding time history plots in Figures 7 and 8.

Glide slope capture following an initial offset in airspeed (4 kt) and vertical position (20 ft) are shown in Tables 5 and 6 respectively. The corresponding time history plots are shown in Figures 9 and 10. The glide slope capture criteria are met with one exception : following an initial offset in airspeed, the vertical position residual error (2.18 ft) slightly exceeds the specified value (2.0 ft), while the maximum throttle excursion (6.30 %) is already above the 6. % limit.

As shown by the frequency response curves in Figure 11, the work-load criterion is not met either : whereas the pitch channel magnitude curve slope (-18.5 dB/decade between 0.4 and 4.0 rad/sec) is quite acceptable, the coresponding slope for the throttle channel (-28.8 dB/decade) is much steeper then the desired -20 dB/decade.

Although the performance criteria were not fully met, the main concern at this point was to improve the work-load metric. To this effect the use of additional sensors to measure higher derivatives of the aircraft outputs was investigated.

TABLE 2

Wind Gust Rejection

RMS Outputs and Controls

STOL - Method II

outputs		3	5	3	design
DLC ?		no	no	yes	criteria
u_a	[ft/sec]	2.22	2.20	2.02	2.25
d	[ft]	5.00	4.79	3.07	6.70
$\dot{d}$	[ft/sec]	1.18	1.13	.974	2.20
δ_t	[%]	2.29	2.26	1.59	3.00
θ	[deg]	.617	.569	.457	2.00

STOL - Method I

outputs		3	5	3	design
DLC ?		no	no	yes	criteria
u_a	[ft/sec]	2.24	2.22	2.04	2.25
d	[ft]	5.44	5.08	3.52	6.70
$\dot{d}$	[ft/sec]	1.29	1.18	1.13	2.20
δ_t	[%]	2.30	2.27	1.59	3.00
θ	[deg]	.648	.578	.483	2.00

TABLE 3

Wind Gust Rejection

Response to a Two-Sigma Horizontal Gust Impulse

STOL - Method I and II

outputs			3	5	3	design
DLC ?			no	no	yes	criteria
u_a	max	[ft/sec]	4.6	4.6	4.6	6.75
d	max	[ft]	2.67	2.43	2.08	20.0
$\dot{d}$	max	[ft/sec]	1.17	1.03	.997	6.50
u_a	residual	[ft/sec]	-.001	-.003	-.032	.675
d	residual	[ft]	.015	.019	.075	2.00
$\dot{d}$	residual	[ft/sec]	-.010	-.011	-.008	.650
δ_t	max	[%]	-.884	-.861	-1.11	6.00
θ	max	[deg]	-.623	-.588	-.443	4.00

TABLE 4

Wind Gust Rejection

Response to a Two-Sigma Vertical Gust Impulse

STOL - Method I and II

outputs			3	5	3	design
DLC ?			no	no	yes	criteria
u_a	max	[ft/sec]	.577	.536	.476	6.75
d	max	[ft]	2.51	2.62	1.68	20.
$\dot{d}$	max	[ft/sec]	1.03	1.10	.829	6.50
u_a	residual	[ft/sec]	.134	.137	.031	.675
d	residual	[ft]	.528	.519	.090	2.00
$\dot{d}$	residual	[ft/sec]	-.055	-.054	-.017	.650
δ_t	max	[%]	-1.61	-1.63	-1.37	6.00
θ	max	[deg]	-.455	-.405	-.356	4.00

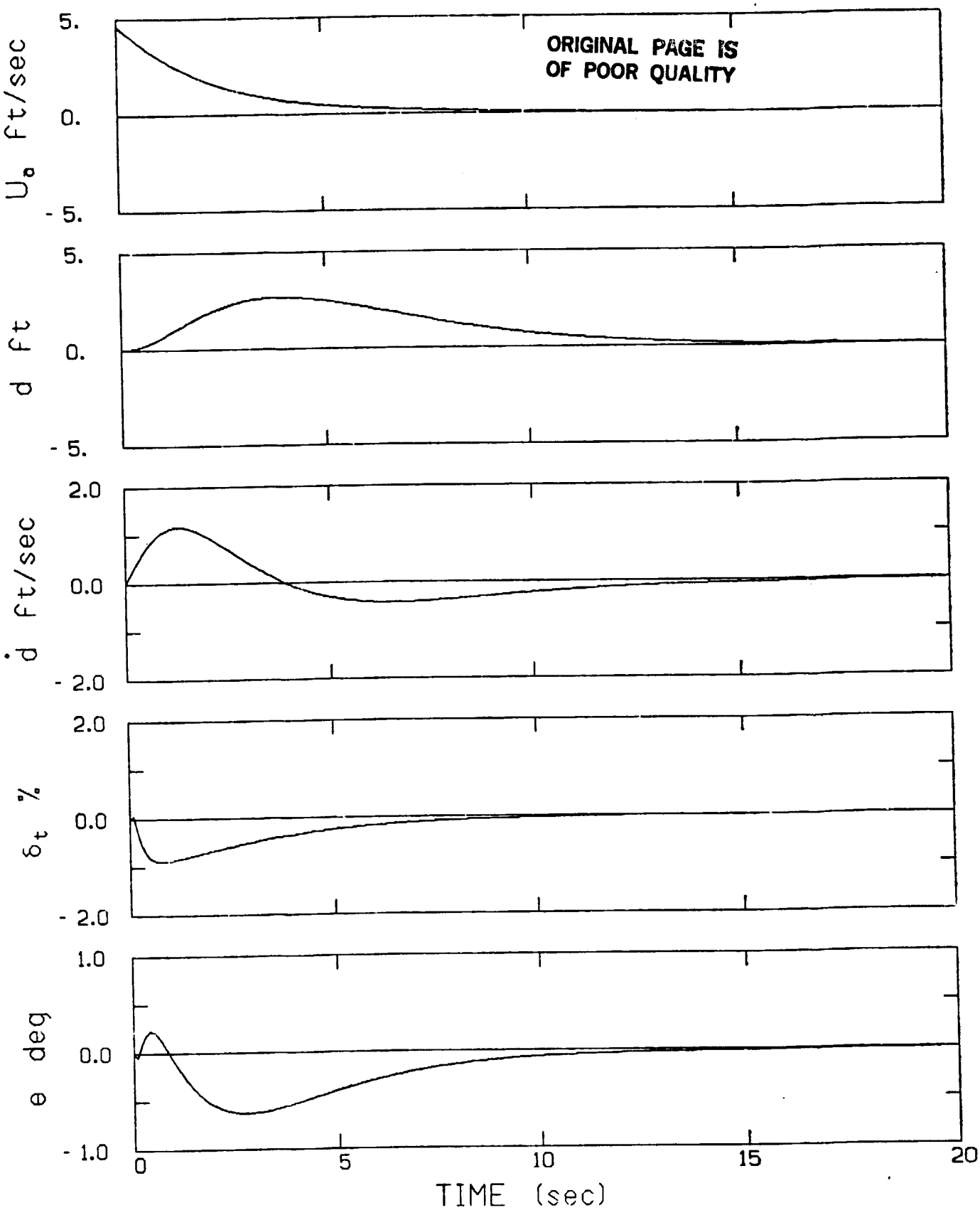

Figure 7: Response to Horizontal Wind Gust (STOL - 3 sensors)

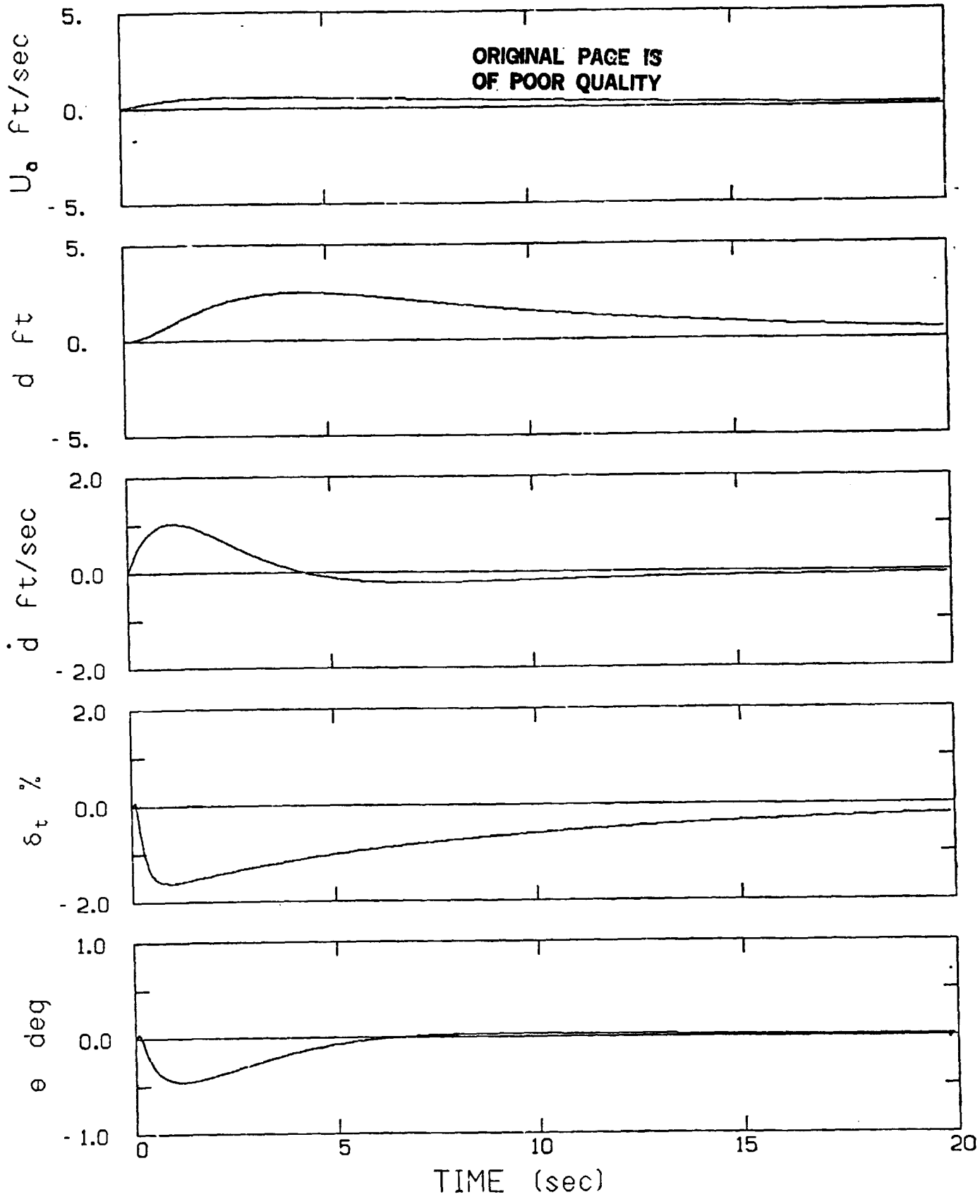

Figure 8: Response to Vertical Wind Gust (STOL - 3 sensors)

TABLE 5

Response to Initial Offset in Airspeed (6.75 ft/sec)

STOL - Method I and II

outputs			3	5	3	design
DLC ?			no	no	yes	criteria
u_a	max	[ft/sec]	6.75	6.75	6.75	6.75
d	max	[ft]	8.83	8.29	5.28	20.0
$\dot{d}$	max	[ft/sec]	3.14	2.83	2.13	6.50
u_a	residual	[ft/sec]	.555	.584	.133	.675
d	residual	[ft]	2.18	2.21	.391	2.00
$\dot{d}$	residual	[ft/sec]	-.229	-.229	-.073	.650
δ_t	max	[%]	-6.30	-6.19	-4.98	6.00
θ	max	[deg]	2.07	1.65	2.23	4.00

TABLE 6

Response to Initial Offset in Vertical Position (20 ft)

STOL - Method I and II

outputs			3	5	3	design
DLC ?			no	no	yes	criteria
u_a	max	[ft/sec]	1.81	1.64	1.37	6.75
d	max	[ft]	20.	20.	20.	20.
$\dot{d}$	max	[ft/sec]	-2.87	-2.64	-3.81	6.50
u_a	residual	[ft/sec]	.430	.436	.102	.675
d	residual	[ft]	1.67	1.65	.298	2.00
$\dot{d}$	residual	[ft/sec]	-.176	-.172	-.056	.650
δ_t	max	[%]	-5.10	-5.16	-2.57	6.00
θ	max	[deg]	-2.83	-2.44	-2.57	4.00

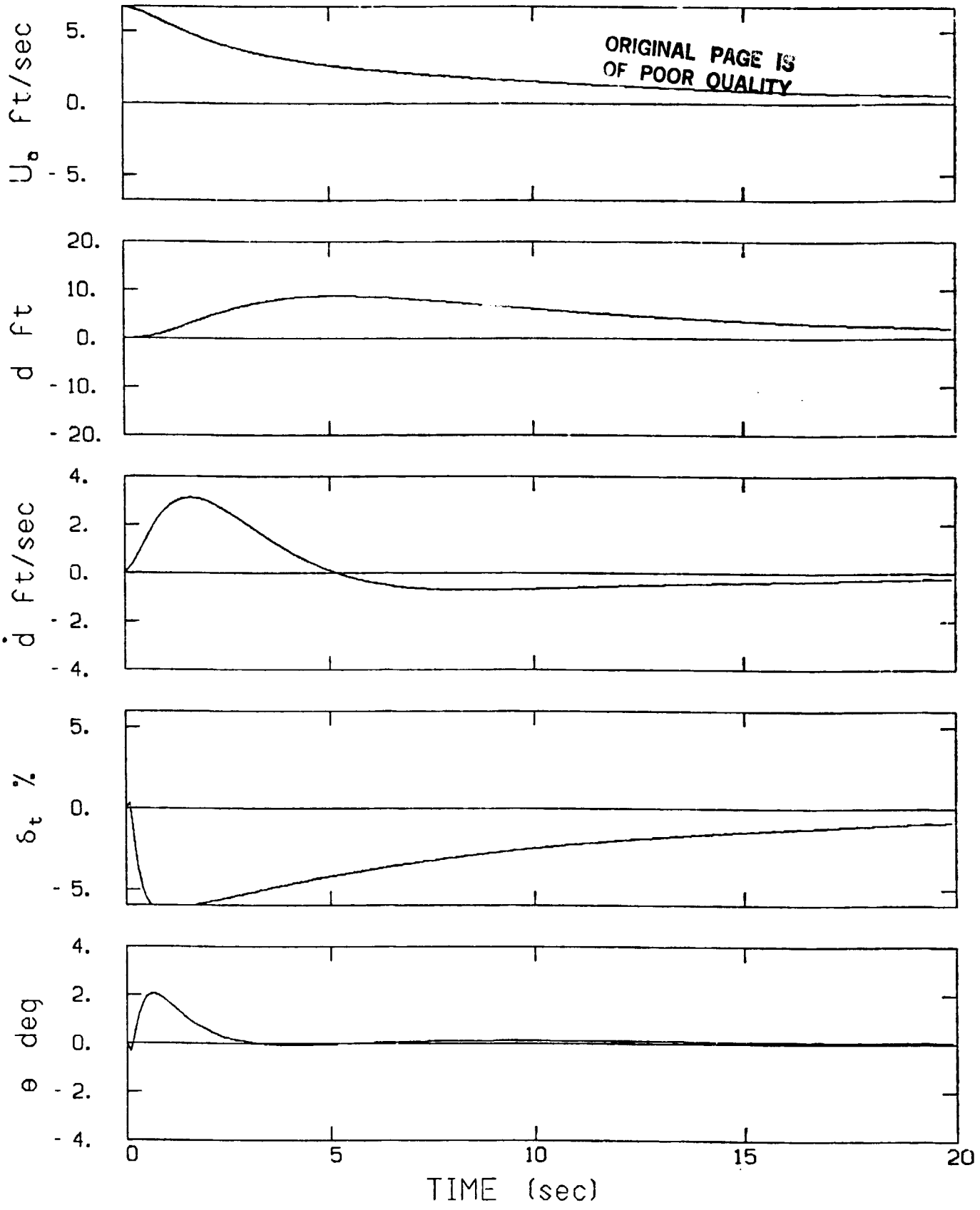

Figure 9: Response to Airspeed Offset (STOL - 3 sensors)

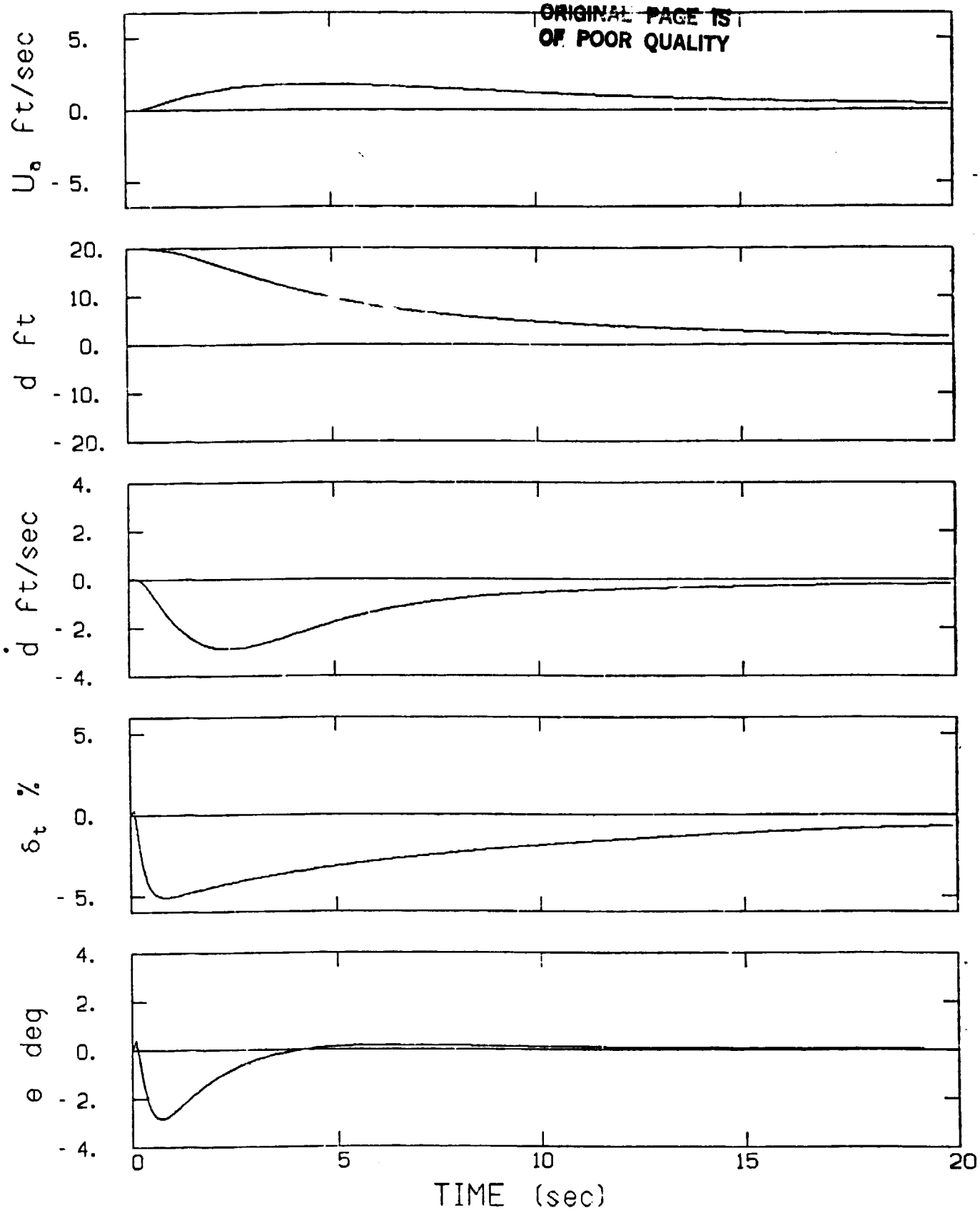

Figure 10: Response to Vertical Position Offset (STOL - 3 sensors)

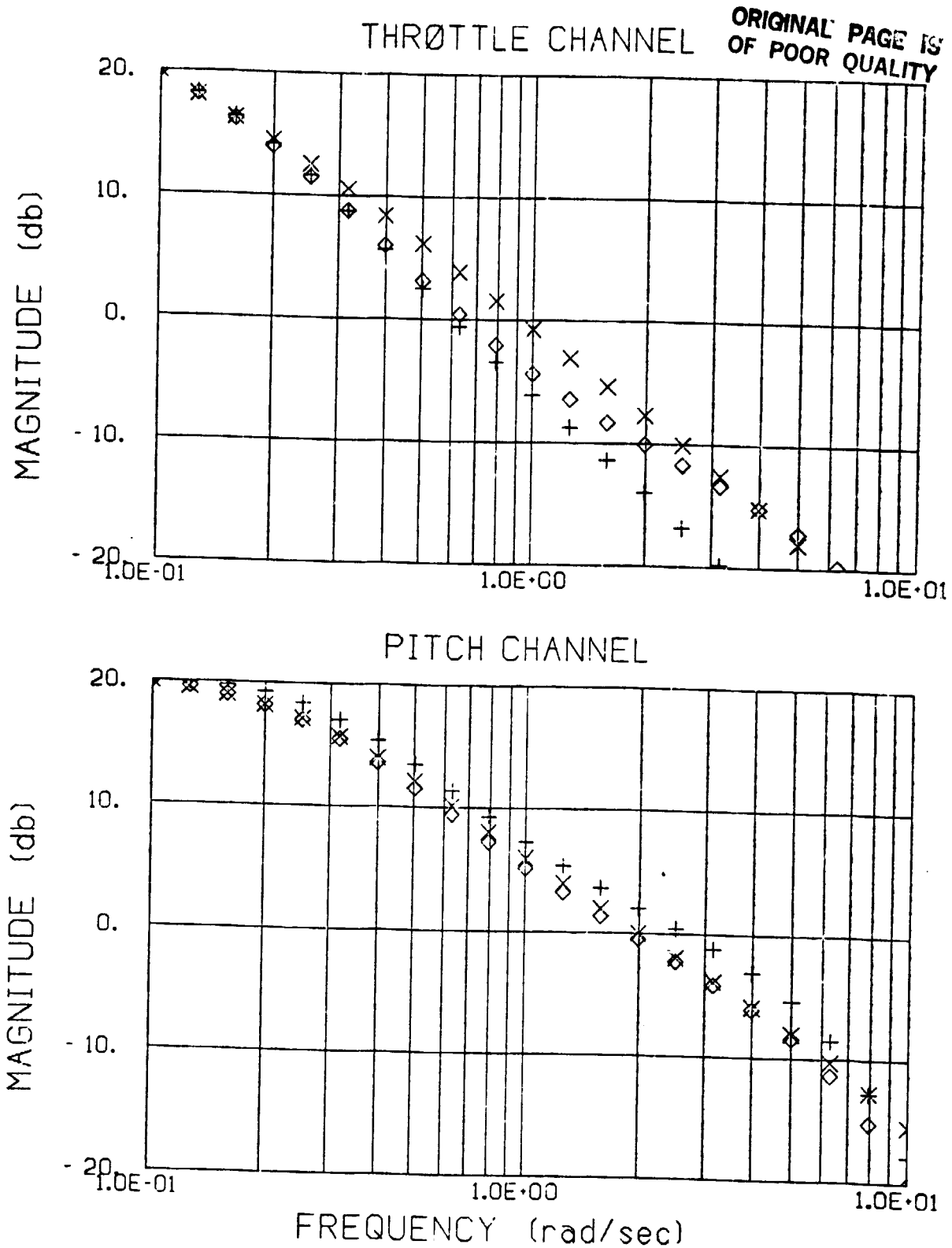

Figure 11: Work-Load Metric (STOL)

6.3.2 Five Sensors Configuration

Adding vertical acceleration ($\ddot{d}$) as the fourth sensor was not sufficient to meet the work-load criterion; and a fifth sensor, axial acceleration ($\dot{u}$) was added as well. Only the two additional output weighting and sensor variances were iterated to obtain the design examples presented below. The objective of these iterations was to improve the work-load metric only, and no attempt was made to improve the performance level. Varying the $\dot{u}$ weighting and sensor noise variance provided a much better control over the magnitude curve slope for the throttle channel than was available in the three sensor configuration. The $\ddot{d}$ weighting was varied mostly to counteract the effect of the $\dot{u}$ weighting on the slope of the pitch attitude magnitude curve.

Wind gust rejection and glide-slope capture performance are shown in the second column of Tables 2 to 6. As expected insufficient throttle effectiveness is still the limiting factor, and the improvement in performance is relatively small (5%-10%). As a result, the corresponding time history plots are not included. On the other hand, Figure 11 shows clearly the improvement in the work-load metric. The frequency response magnitude curve slope is -19.9 dB/decade (between 0.4 and 4.0 rad/sec) for the pitch attitude channel. The corresponding slope for the throttle channel is -23.7 dB/decade, quite close to the desired value of -20. dB/decade.

6.3.3 DLC Configuration (with 3 sensors)

The results presented so far, especially for the glide-slope capture, clearly indicate that performance is limited by the available throttle authority. Consequently, the use of the DLC mode where the spoilers are linked to the throttle was investigated. The spoilers to throttle ratio was chosen to effectively double the throttle authority (c.f., Appendix A for the values of Z_{sp} versus Z_e, and X_{sp} versus X_e). The spoiler actuators are also very fast, thereby partially compensating for the more sluggish thrust response of the engine. The loss of maximum usable lift is acceptable in view of the substantial stall margin of the QSRA. It should be noted that the DLC mode is part of the original design of the aircraft, and its usefulness has been proven in flight. In particular, during carrier trials of the QSRA by the Navy [17], the DLC mode was instrumental in bringing the pilot's work-load down to acceptable levels (no flight director was used).

The improvement in performance is quite dramatic, as shown in the third column of Tables 2 to 6. The corresponding time history plots are presented in Figurs 12 to 15. The work-load metric is shown in Figure 11. The average slopes of the frequency response magnitude curves are -19.7 and -21.5 dB/decade for the pitch attitude and the throttle channels respectively (between 0.4 and 4.0 rad/sec).

Last but not least, the above results were obtained using only three sensors, thereby simplifying the flight director implementation in the aircraft. This indicates that the faster acting spoilers, used in the DLC mode, reduce the need for lead equalization so that sensors to

measure higher derivatives of the aircraft's states are not required. As all design criteria were improved, no further iterations were performed. The cost function weighting matrices are the same as those used in the three sensors configuration presented in Section 6.2.1.

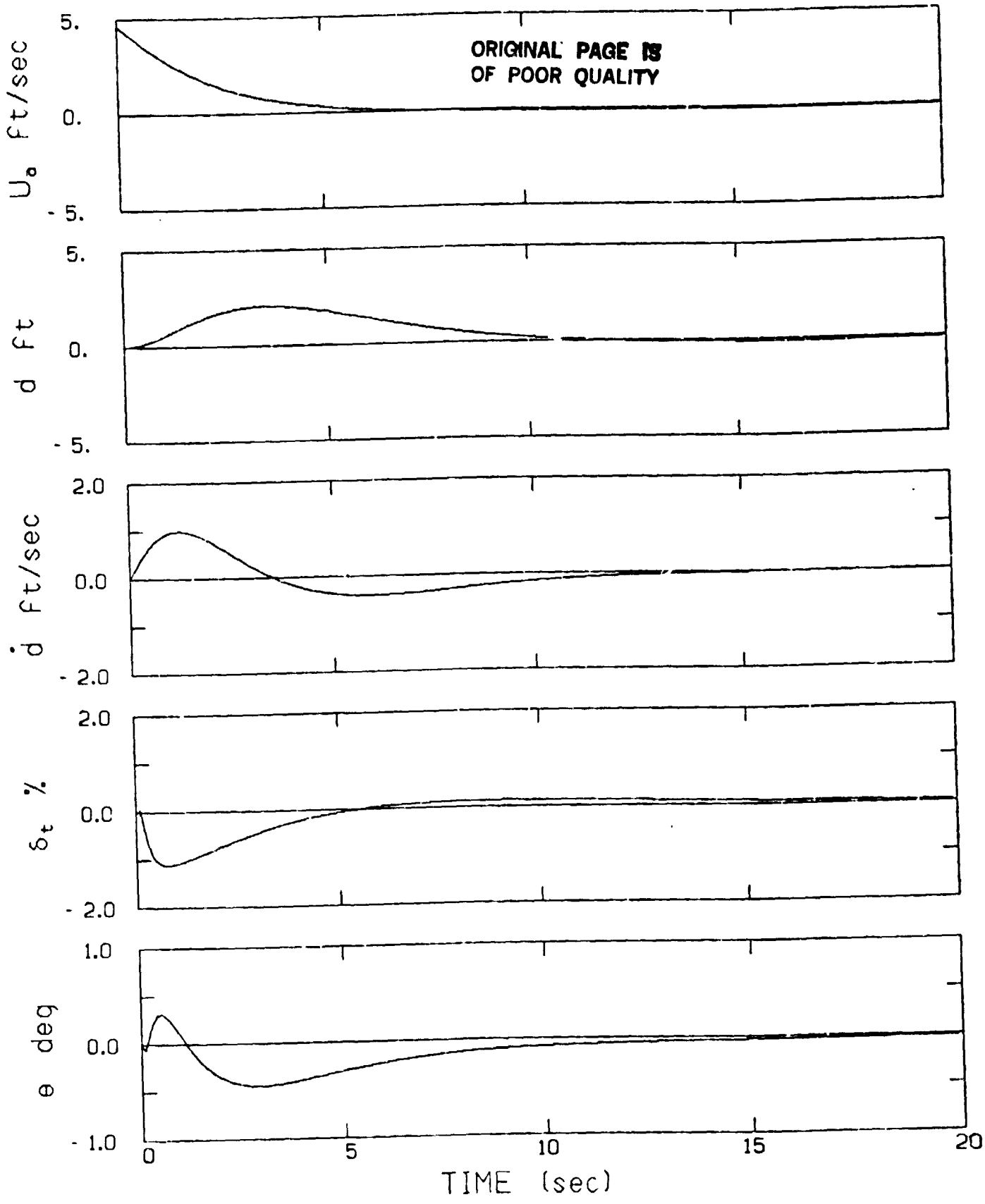

Figure 12: Response to Horizontal Wind Gust (STOL - DLC)

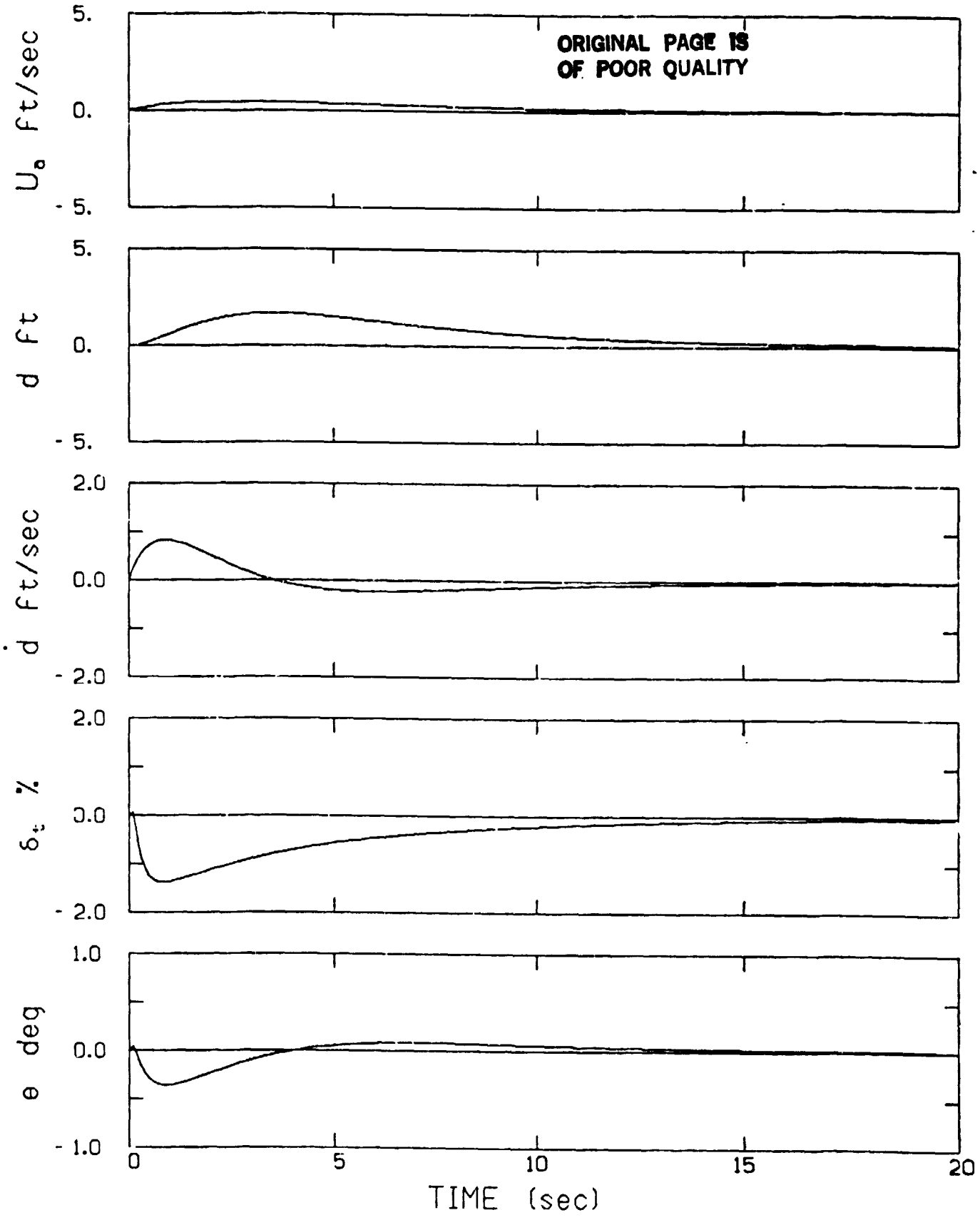

Figure 13: Response to Vertical Wind Gust (STOL - DLC)

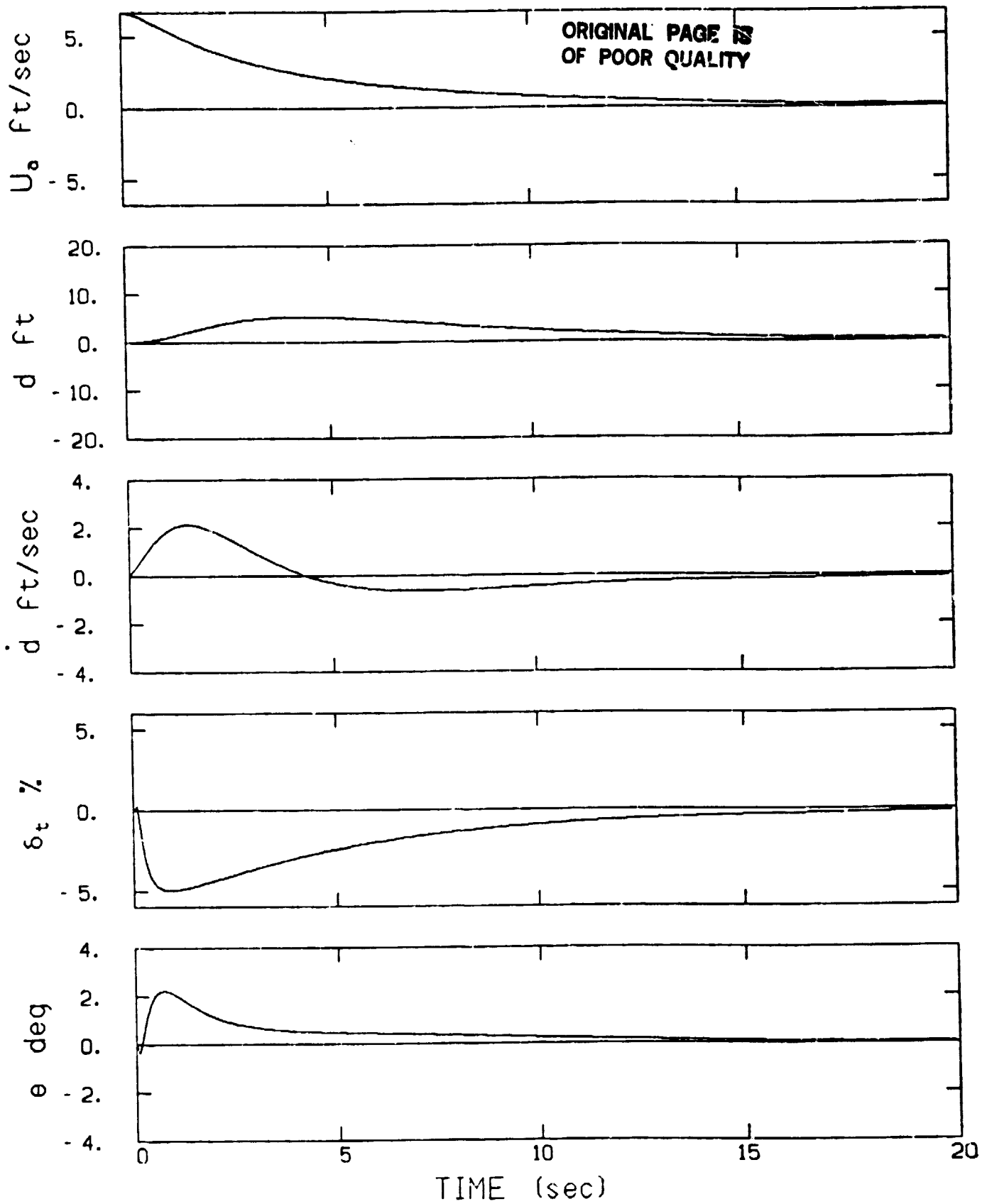

Figure 14: Response to Airspeed Offset (STOL - DLC)

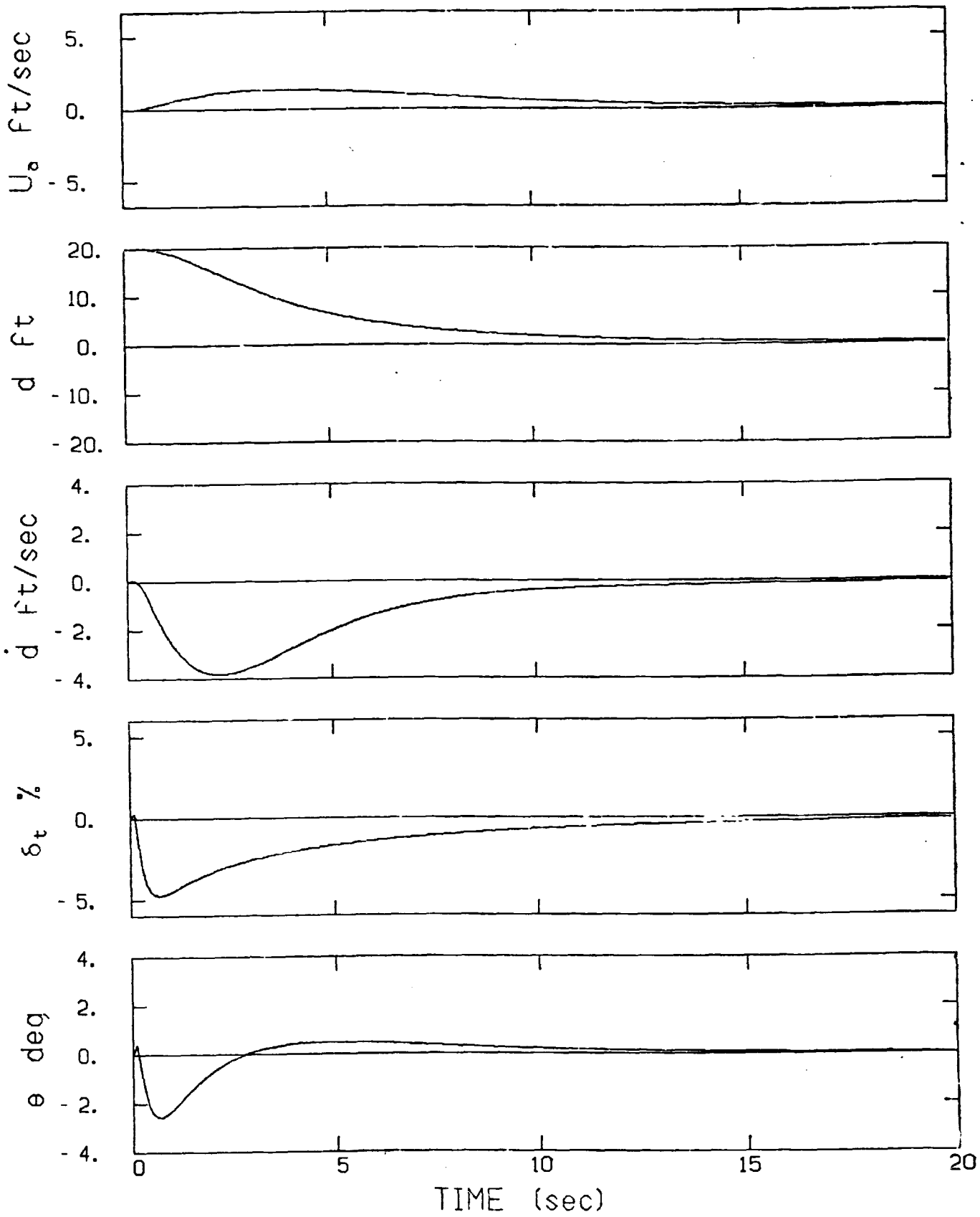

6.4 C/STOL CONFIGURATION

The C/STOL configuration (c.f., Section 3.3) represents the transition between the conventional and the STOL configurations. The USB flaps are partially deflected to 30 degrees. Following the trade-off study results, DLC is used with three aircraft sensors. As this configuration is not as highly coupled as the STOL one, the value chosen for the DLC gain is only half of that used previously. Thus, a two percent increase in throttle will result in a one degree decrease in spoiler deflection.

The results, presented in Tables 7 and 8, and in Figures 16 to 18, are similar to those of the STOL configuration with DLC.

TABLE 7

Wind Gust Rejection

RMS Outputs and Controls

C/STOL Configuration

method		I	II
u_a	[ft/sec]	2.15	2.13
d	[ft]	3.01	2.81
$\dot{d}$	[ft/sec]	.940	.872
δ_t	[%]	1.54	1.53
θ	[deg]	.563	.559

TABLE 8

Wind Gust Rejection and Glide-Slope Capture

C/STOL - Method I and II

criterion			u_W	w_W	u_0	w_0
u_a	max	[ft/sec]	4.6	.688	6.75	1.88
d	max	[ft]	2.19	1.68	5.17	20.0
$\dot{d}$	max	[ft/sec]	1.06	.859	2.14	-4.79
u_a	residual	[ft/sec]	-.075	.084	.306	.190
d	residual	[ft]	-.113	.156	.567	.352
$\dot{d}$	residual	[ft/sec]	.006	-.024	-.087	-.054
δ_t	max	[%]	-.879	-1.38	-4.73	-3.82
θ	max	[deg]	-.415	-.616	1.66	-3.52

where

u_W : response to horizontal gust impulse

w_W : response to vertical gust impulse

u_0 : response to initial offset in airspeed

w_0 : response to initial offset in vertical position

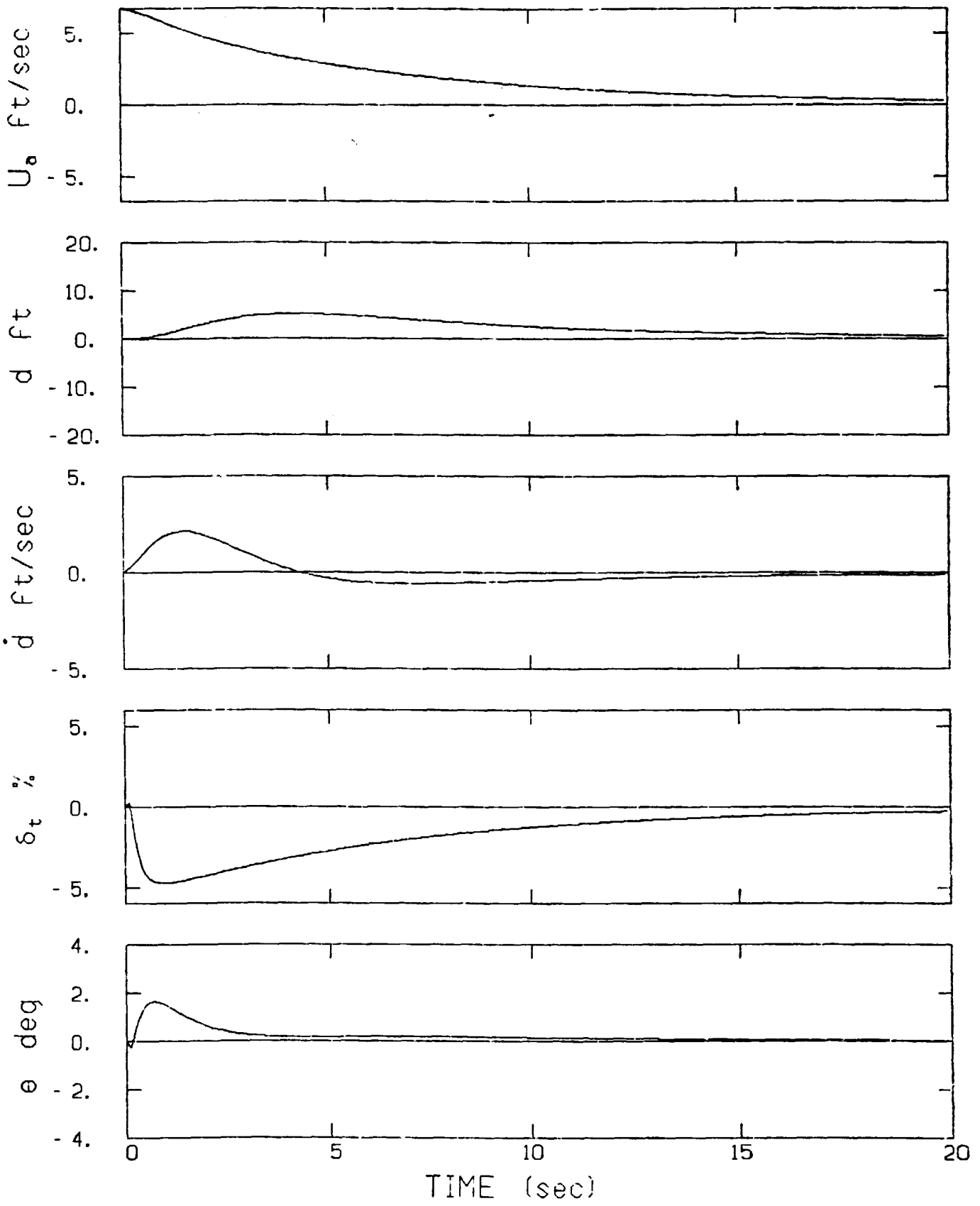

Figure 16: Response to Airspeed Offset (C/STOL)

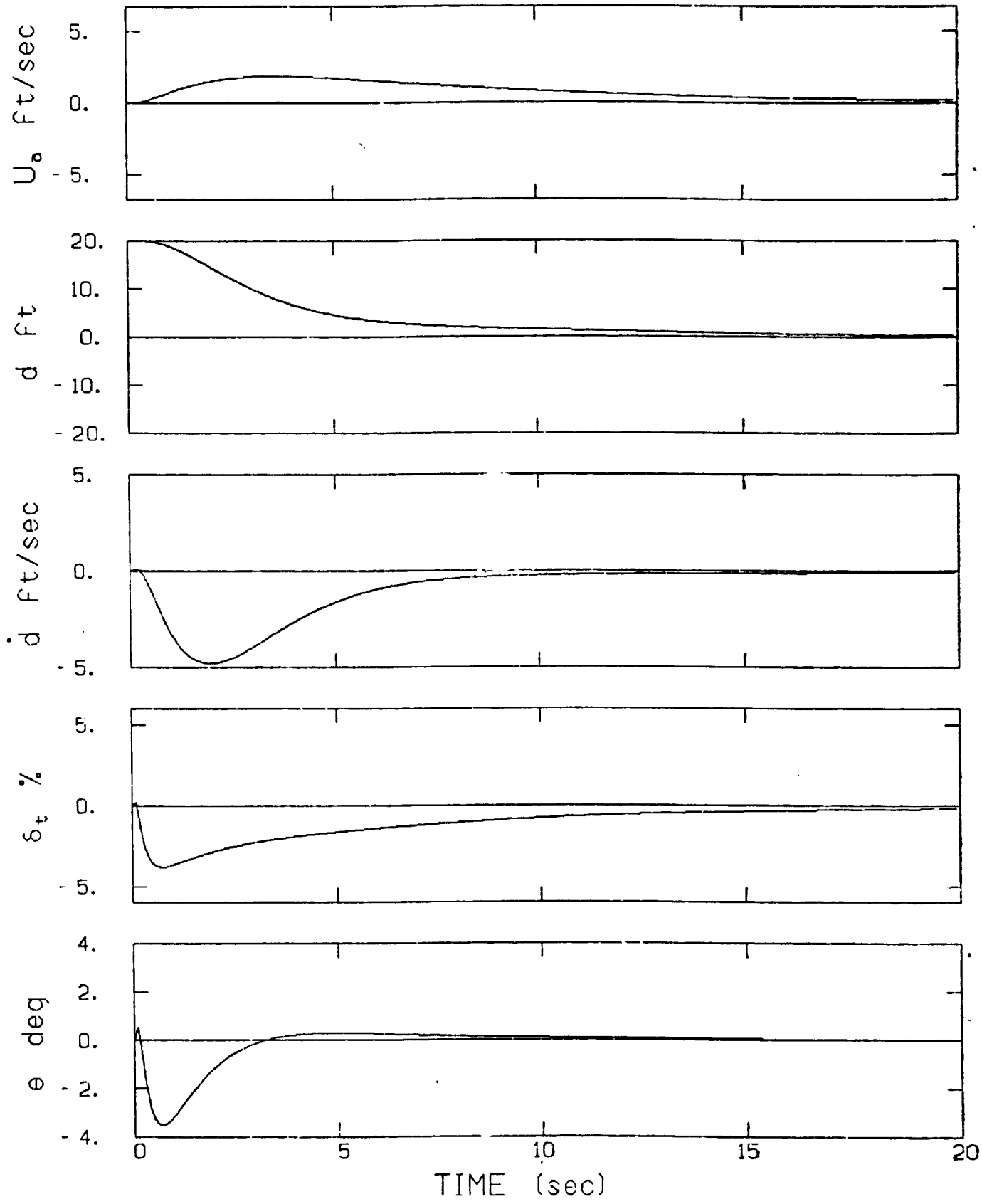

Figure 17: Response to Vertical Position Offset (C/STOL)

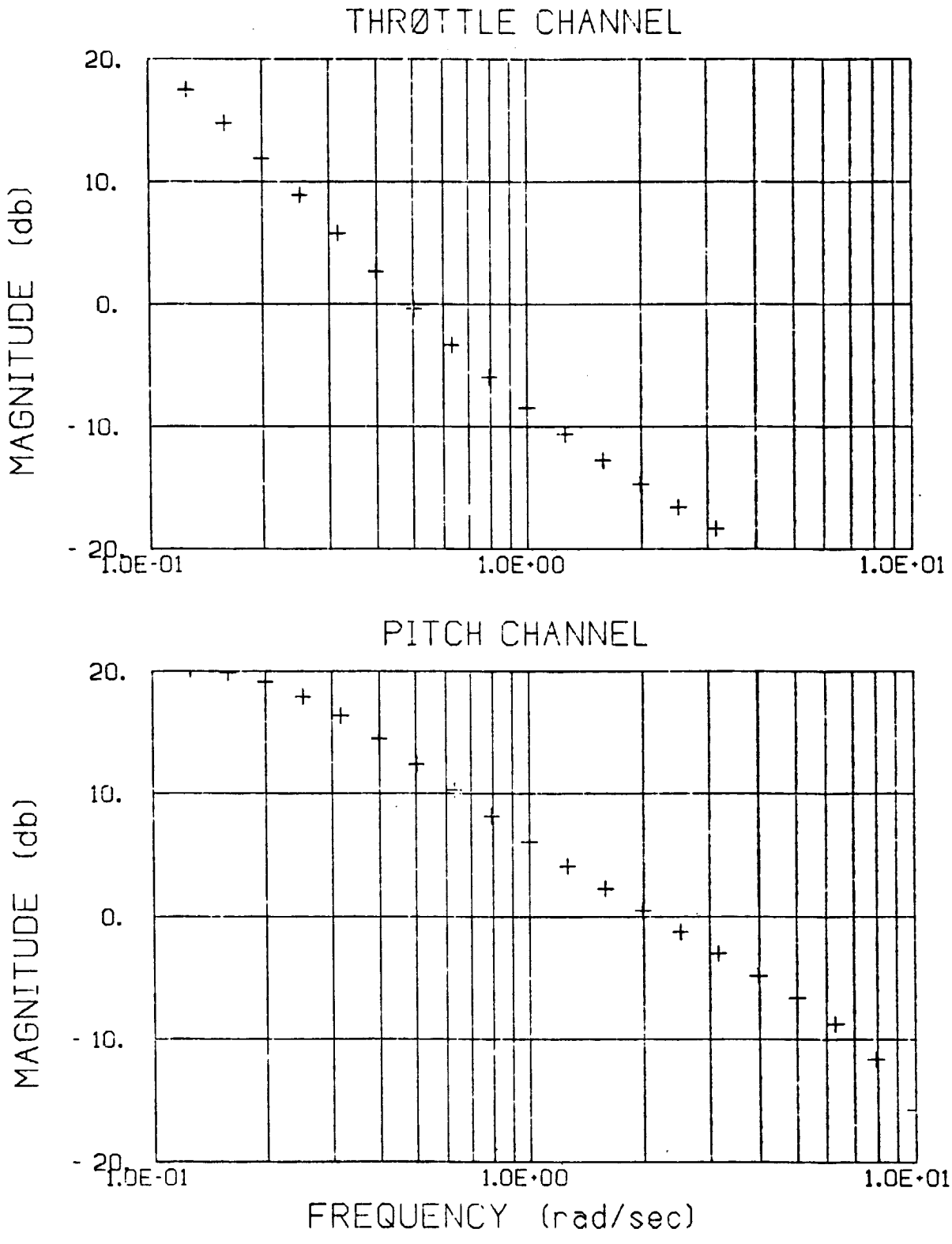

Figure 18: Work-Load Metric (C/STOL)

Chapter VII

CONCLUSIONS AND RECOMMENDATIONS FOR FUTURE RESEARCH

7.1 CONCLUSIONS

Two methods for flight director control law design have been presented. The first design method, proposed by Levinson, is based directly on the OCM concept. The second design method, proposed here, uses a fixed dynamic model of the pilot in a state space formulation similar to that of the OCM. The second design method also includes an explicit work-load metric.

The several design examples presented in Chapter VI, clearly show the strong impact of throttle effectiveness on the performance and pilot work-load associated with manual control of a powered-lift STOL aircraft during approach. Use of DLC to increase throttle effectiveness greatly improves performance and reduces pilot work-load.

Flight path regulation in the presence of turbulence, initial capture of the glide-slope, and acceptable response to horizontal windshear, can be achieved, equally well, by both methods.

The two design methods have the following features in common:

1. They are based on a highly structured state space pilot/vehicle model, and use a Kalman-filter/LQ regulator. Their use requires

less expertise and engineering judgment than classical manual control design methods.

2. The special requirements of the OCM concerning pilot observation and motor noise-to-signal ratios can be easily achieved.

3. Only three aircraft sensors were required to achieve the desired performance.

Design method II has the following advantages over method I :

1. An explicit work-load metric is included, which should improve the suitability of the flight director for manual control tasks. This metric is affected by the throttle effectiveness, and by the number of sensors used. With DLC only three sensors were necessary; without DLC, two additional sensors were required to achieve the desired work-load level. Thus, a minimum sensor complement can be determined early in the design process which is not the case for method I. Iterating the weighing matrices and sensor noise levels to meet the work-load criterion has only a small effect on the flight director performance. Hence, the flight director can be designed in two consecutive phases : (1) performance improvement, and (2) work-load reduction.

2. A simpler model of the pilot's observation and scanning process is required. The complexity of the observation model increases with the number of controls for the second design method whereas it increases with the number of outputs for the first method.

Also, the pilot's observation model used in method I is not relevant to the actual control task. The resulting control laws may have to be revised to account for the difference between the pilot observation noise levels used in the design phase and the actual sensor noise levels.

3. The second method is more flexible in tnat any linear model of the pilot can be used, whereas the first method is limited to the OCM. Improved models of the human operator can be incorporated in the future with only a few modifications.

7.2 RECOMMENDATIONS FOR FUTURE RESEARCH

Design methods I and II should be evaluated in a piloted simulation. Of particular interest are :

1. Pilot opinion ratings for the two methods.

2. The performance levels achieved in the simulator as compared to those predicted by the two design methods.

3. The correlation between the work-load metric proposed for method II and pilot opinion ratings. This could be done by comparing pilot opinion ratings for the three design examples presented in Chapter VI, or by generating additional examples with varying levels of work-load. In addition to validating the proposed metric, these data could be used as guidelines for simplifying the flight director control laws.

4. The robustness of the design to variations in the pilot model parameters : time delay, neuromuscular time constant, and pilot observation noise levels.

REFERENCES

1. Franklin, J.A. and Innis, R.C., "Flight-Path and Airspeed Control During Landing Approach for Powered-Lift Aircraft", NASA TN D-7791, October 1974.

2. McCracken, R.C., "Quiet Short-Haul Research Aircraft Familiarization Document", NASA TM-81149, November 1979.

3. Flora, C.C., Middleton, R. and Schaer, D.K., "Quiet Short-Haul Research Aircraft Predicted Flight Characteristics", NASA CR-152203, October 1979.

4. McRuer, D.T. and Krendel, E.S., "Mathematical Models of Human Pilot Behavior", NATO AGARDograph No. 188, January 1974.

5. McRuer, D.T., Graham, D., Krendel, E. and Reisener, W., "Human Pilot Dynamics in Compensatory Systems - Theory, Models, and Experiments with Controlled Element and Forcing Functions Variables," AFFDL-TR-65-15, January 1965.

6. Kleinman, D.L., Baron, S. and Levinson, W.H., "An Optimal-Control Model of Human Response, Part I : Theory and Validation", Automatica, Vol. 6, pp. 357-369, 1970.

7. Levinson, W.H., Baron, S. and Kleinman, D.L., "A Model for Human Controller Remnant", IEEE, Trans. Man-Machine Systems, Vol. MMS-10, No. 4, December 1969.

8. Kleinman, D.L. and Baron, S., "Manned Vehicule Systems Analysis by Means of Modern Control Theory", NASA CR-1753, June 1971.

9. Hess, R.A., "Application of a Model-Based Flight Director Design Technique to a Longitudinal Hover Task", AIAA, Journal of Aircraft, Vol. 14, No. 3, pp. 265-271, March 1977.

10. Levinson, W.H., "A Model-Based Technique for the Design of Flight Directors", Proc. Ninth Annual Conference on Manual Control, May 1973.

11. Baron, S. and Levinson, W.H., "Display Analysis with the Optimal Control Model of the Human Operator", Human Factors, Vol. 19, No. 5, pp. 437-457, October 1977.

12. Bryson, A.E. and Ho, Y.C., Applied Optimal Control, Hemisphere Pub. Co., Washington, D.C., 1975.

13. Bryson, A.E. and Hall, W.E., "Optimal Control and Filter Synthesis by Eigenvector Decomposition ", Stanford University Department of Aeronautics and Astronautics Report No. 436, December 1971.

14. Holley, W.E. and Bryson, A.E., "Wind Modeling and Lateral Control for Automatic Landing," J. Spacecraft, Vol. 14, No. 2, pp. 65-72, February 1977.

15. Baron, S. and Levinson, W.H., "A Manual Control Theory Analysis of Vertical Situation Display for STOL Aircrafts," NASA CR-114620, April 1973.

16. Hindson, W.S., Hardy, G.H. and Innis, R.C., "Flight-Test Evaluation of STOL Control and Flight Director Concepts in a Powered-Lift Aircraft Flying Curved Decelerating Approaches," NASA TP-1641, March 1981.

17. Queen, S. and Cochrane, J., "Quiet Short-Haul Research Aircraft Joint Navy/NASA Sea Trials", J. Aircraft, Vol. 19, No. 8, pp.655-660, August 1982.

Appendix A

MODEL PARAMETERS FOR THE QSRA

configuration		STOL	C/STOL	CTOL
U_0	[kt]	70.	90.	130.
h	[ft]	500.	1000.	1000.
γ_0	[deg]	-6.	-6.	0.
δ_{usb}	[deg]	50.	30.	0.
X_u	[sec^{-1}]	-.074	-.066	-.06
X_w	[sec^{-1}]	.131	.1056	.094
X_e	[$ft/sec^2/\%$]	.031	.067	.22
X_{sp}	[$ft/sec^2/deg$]	.034	.012	
Z_u	[sec^{-1}]	-.365	-.304	-.21
Z_w	[sec^{-1}]	-.485	-.547	-.862
Z_e	[$ft/sec^2/\%$]	-.327	-.293	-.22
Z_{sp}	[$ft/sec^2/deg$]	-.298	-.506	
$1/T_u$	[sec^{-1}]	.3	.237	.342
$1/T_w$	[sec^{-1}]	.73	.532	.768
Q_u	[ft^2sec^{-1}]	35.	45.	31.
Q_w	[ft^2sec^{-1}]	14.	19.9	13.7